TECHNICAL UNIVERSITY OF LIBEREC
Faculty of Mechanical Engineering

Piezoelectric film sensors for the cavitation impact measurement

Master Thesis

Study programme:	N2301 Mechanical Engineering
Study branch:	Machines and Equipment Design
Author:	**Menghuot Phan**
Thesis Supervisors:	Ing. Miloš Müller, Ph.D. Department of Power Engineering Equipment

Liberec 2020

TECHNICKÁ UNIVERZITA V LIBERCI
Fakulta strojní

Zadání diplomové práce

Piezoelectric film sensors for the cavitation impact measurement

Jméno a příjmení:	**Menghuot Phan**
Osobní číslo:	S18000211
Studijní program:	N2301 Mechanical Engineering
Studijní obor:	Machines and Equipment Design
Zadávající katedra:	Katedra energetických zařízení
Akademický rok:	**2019/2020**

Zásady pro vypracování:

- A review of methods used for the production of piezoelectric sensors for the cavitation impact measurements with the special focus on thin film sensors
- Fundamental properties of piezoelectric film sensors towards the cavitation impact measurement
- The elaboration of a methodology for the production of piezoelectric sensors for the cavitation impact measurement
- Design and production of piezoelectric film sensors of different sizes and configurations for the cavitation impact measurement
- The tensing of an appropriate cover for the sensor protection
- The calibration of the sensors using an appropriate method
- The application of sensors for the measurement of the acoustic cavitation

Rozsah grafických prací: 10
Rozsah pracovní zprávy: 50
Forma zpracování práce: tištěná/elektronická
Jazyk práce: Angličtina

Seznam odborné literatury:

1. KIM, Ki-Han, Georges CHAHINE, Jean-Pierre FRANC a Ayat KARIMI. *Advanced experimental and numerical techniques for cavitation erosion prediction*. Dordrecht: Springer, [2014]. Fluid mechanics and its applications, v. 106.
2. FRANC, Jean-Pierre a Jean-Marie MICHEL. *Fundamentals of cavitation*. Boston: Kluwer Academic Publishers, c2004. ISBN 1402022328.
3. BRENNEN, Christopher E. *Cavitation and bubble dynamics*. New York: Cambridge University Press, c2014. ISBN 978-1-107-64476-2.
4. SOYAMA, Hitoshi, MOMMA Takahiro, LICHTAROWICZ Andrzej and Edward WILLIAMS. *A New Calibration Method for Dynamically Loaded Transducers and Its Application to Cavitation Impact Measurement*. Journal of Fluids Engineering. 1998, 120(4). 10.1115/1.2820728.
5. CONG, Jiqing, Jianping JING, Changmin CHEN a Zezeng DAI. *Development of a PVDF Sensor Array for Measurement of the Dynamic Pressure Field of the Blade Tip in an Axial Flow Compressor*. Sensors (Basel, Switzerland). 2019Mar, 19(6): 1404. DOI: 10.3390/s19061404.

Vedoucí práce: Ing. Miloš Müller, Ph.D.
Katedra energetických zařízení

Datum zadání práce: 1. listopadu 2019
Předpokládaný termín odevzdání: 30. dubna 2021

prof. Dr. Ing. Petr Lenfeld
děkan

Technická univerzita v Liberci
FS
-8-

doc. Ing. Petra Dančová, Ph.D.
vedoucí katedry

V Liberci dne 14. února 2020

Declaration

I hereby certify, I, myself, have written my master thesis as an original and primary work using the literature listed below and consulting it with my thesis supervisor and my thesis counsellor.

I acknowledge that my bachelor master thesis is fully governed by Act No. 121/2000 Coll., the Copyright Act, in particular Article 60 – School Work.

I acknowledge that the Technical University of Liberec does not infringe my copyrights by using my master thesis for internal purposes of the Technical University of Liberec.

I am aware of my obligation to inform the Technical University of Liberec on having used or granted license to use the results of my master thesis; in such a case the Technical University of Liberec may require reimbursement of the costs incurred for creating the result up to their actual amount.

At the same time, I honestly declare that the text of the printed version of my master thesis is identical with the text of the electronic version uploaded into the IS/STAG.

I acknowledge that the Technical University of Liberec will make my master thesis public in accordance with paragraph 47b of Act No. 111/1998 Coll., on Higher Education Institutions and on Amendment to Other Acts (the Higher Education Act), as amended.

I am aware of the consequences which may under the Higher Education Act result from a breach of this declaration.

June 11, 2020

Menghuot Phan

ABSTRACT

Piezoelectric sensors based on the thin piezoelectric polyvinylidene fluoride (PVDF) polymer films are developed and fabricated to measure the interaction magnitude between the cavitating field and the material surface. In this thesis, PVDF sensors ware fabricated by photolithography processes. Kapton tape was tested to protect the sensors from the cavitation damage. The sensors developed within the thesis and commercial variants of the sensors were compared and analyzed. The drop ball calibration technique was used to set the sensitivity of the sensors to the impact forces. Four different ball-masses three and different drop heights were tested during the calibration. The relationship between the time duration of the signal generated by the sensors and the initial drop high in the calibration method was also analyzed. The different sizes and protective layer configurations of the PVDF sensor were prepared and tested. The developed PVDF sensor was successfully applied to the measurement of the acoustic cavitation field generated by ultrasonic horn proving higher sensitivity than commercial variant.

Keywords: cavitation, collapse, PVDF sensor, photolithography.

ACKNOWLEDGEMENTS

I would like to express my sincere gratitude to my supervisors, Ing. Miloš Müller, Ph.D., for valuable advice, encouragement, and guidance during this thesis. Moreover, I would like to convey my thankfulness to Ing. Jan Hujer, Ph.D., for his assistance in the experiment.

This work was supported by the Student Grant Competition of the Technical University of Liberec under project No. SGS-2020-5028.

Menghuot Phan

TABLE OF CONTENTS

LIST OF FIGURES

LIST OF TABLES

LIST OF SYMBOLS AND ABBREVIATIONS

Symbol	Description	Unit
A	Area	$[m^2]$
C	Capacitance	[F]
d	Piezo strain constant	$[(m/m)/(V/m)^{-1}]$
D	Electric displacements	$[C/m^2]$
E	Electric field component	[V/m]
F_{max}	Maximum force	[N]
F_{mean}	Mean impact force	[N]
g	Acceleration due to gravity	$[m/s^2]$
h	Height	[m]
R	Bubble radius	[m]
P	Pyroelectric coefficient	$[C/m^2\ K]$
P_v	Vapor pressure of the liquid	[Pa]
P_∞	liquid pressure at an infinite distance from the bubble	[Pa]
P_i	Pressure inside the bubble	[Pa]
R(t)	Bubble radius as a function of time	[m]
$\dot{R}$	First order derivative of bubble radius	[m/s]
$\ddot{R}$	Second order derivative of bubble radius	[m/s]
R_0	Initial bubble radius	[m]
t	Time	[s]
T	Temperature	[K]
S	Surface tension coefficient	[N/m]
U_{max}	Maximum voltage	[V]
v	Velocity	[m/s]
τ	Rayleigh time	[s]
τ	Impact duration time	[s]
γ	Polytropic exponent of the gas	[-]
μ	Dynamic viscosity	[Pa.s]
ε	Permittivity	[F/m]
ε_r	Relative permittivity	[-]

ε_0	permittivity of free space, 8.854 x 10^{-12} F/m	[F/m]
ρ_m	Mass Density	[kg/m^3]
ρ_e	Volume Resistivity	[Ωm]
ρ	Density of the liquid	[kg/m^3]

List of Abbreviations

DAQ	Data acquisition
DC	Direct Current
PVDF	Polyvinylidene Fluoride
MSI	Measurement Specialties Inc.
NI	National Instruments
TUL	Technical University of Liberec

1 INDRODUCTION

The cavitation phenomenon consists of the formation, evaluation, and collapse of gas or vapor bubbles. It will occur in liquid phases below static pressure gradients as well as in flowing liquids. Cavitation is responsible for issues such as erosion of solid surfaces in contact with the liquid, noise, and vibration. The presence of cavitation can result in an improper function of a hydraulic systems turbines, pumps, valves, hydrofoils, or drag reduction of ship propellers. The loss of materials is known in the literature as the cavitation erosion. However, in some particular cases, cavitation also has a positive effect. For instance, in the case of submarine vehicles, or the break of kidney stones in shock wave lithotripsy in the field of medicine. Cavitation can also be used for the ultrasonic cleaning of wastewater.

The erosion damage and the magnitude of the cavitation loading on the surface are important factors for the cavitation prediction. Many researchers have developed special transducers that are able to measure the interaction between the cavitation field and the surface with a high resonance frequency over a short duration. An important group of the transducers are piezoelectric film sensors capable to measure the impact forces generated during the interaction between the cavitation field and the wall. The film sensors are flexible so they can be easily shaped and have high mechanical resistance.

1.1 Cavitation

1.1.1 Definition of Cavitation

Cavitation can be explained as the breakdown of a liquid medium under very low pressures [1]. This makes cavitation connect to the field of continuum mechanics, and it applies to both cases whether the liquid is either static or in motion. Cavitation behavior can be described by the phase diagram of water, as shown in Figure 1.1. A curve separates liquid and vapor from the triple point Tr to the critical point Cr. From Figure 1.1, the liquid can be changed to vapor in two different ways. One of which is keeping constant pressure while increasing the temperature known as boiling and another is lowering the pressure while having a constant temperature. At this time, the liquid will change to vapor as cavitation [2]. The explanation of cavitation above is just valid in static conditions when the liquid is in contact with its vapor through the presence of a free surface. In real flow conditions as in rotating machines, the vaporization of liquid can only occur through the presence of small

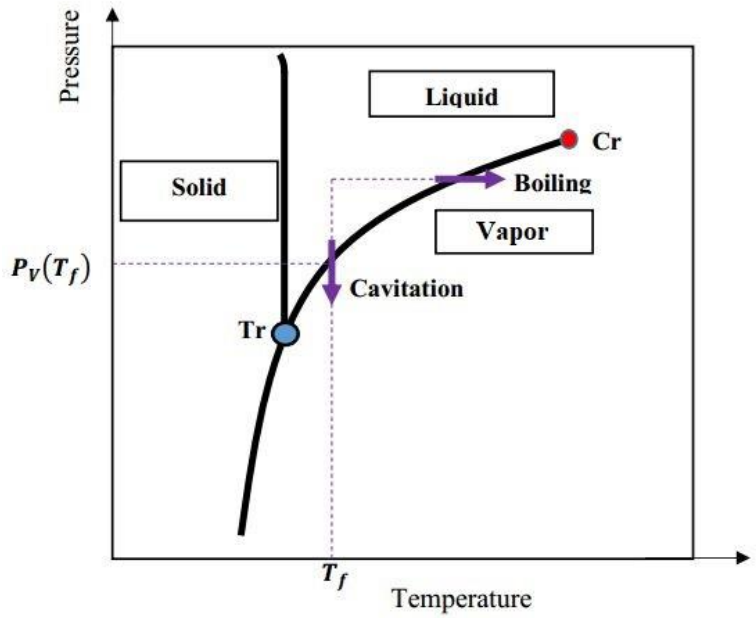

Figure 1.1:Phase diagram of water [33].

bubbles, also noted nuclei. Bubbles sized from the nucleation process are usually around 5 μm to 100 μm. When the nuclei are formed as a result of the intermolecular interaction, the phenomenon is called homogeneous nucleation. Furthermore, when the cavities are formed by the interaction of the molecules with the solid surface, it is known as heterogeneous nucleation.

1.1.2 Classification of Cavitation

Cavitation can be classified for example according to the bubble content to vaporous cavitation and gaseous cavitation. Vaporous cavitation can occur in the fluid flow where the local static pressure drops under the saturated vapor pressure at local temperature. The local pressure decrease can be caused by the local liquid acceleration or by the pulsating acoustic field. The gaseous cavitation occurs when the local static pressure drops under the saturation pressure of the no condensable gas resolved in the liquid. The amount of the gas which can be resolved in the liquid under a given pressure is given by Henry's law. Note that the vapor production with the increase in temperature under constant pressure is called boiling.

Hydrodynamic cavitation is produced by pressure reduction of flowing liquid, such as in ship propellers, pumps, turbines, hydrofoils, and nozzles when the system velocity varies. It is generally happening at lower frequencies, approximately 1-20 kHz. Hydrodynamic cavitation can be divided into several groups.

The traveling cavitation occurs by individual transient cavities or bubbles that form in the liquid, expand or shrink, and then collapse [3]. This type of cavitation can be observed on hydrofoils at tiny angles of attack. In so called fixed cavitation, the fluid flow close to the solid boundary separates from the solid surface and bubbles formed in a cavitation zone attached to the surface, form a large cavity in a quasi-steady sense [4]. Generally, it arises in high temperature boiling of the turbulent zone and can be found after inception has occurred. The vortex cavitation is indicated in the core of vortices in regions of high shear. It is seen in tip vortices trailing from a propeller [5].

Acoustic cavitation is developed with strong ultrasound as a result of pressure changes of cyclic ultrasonic waves in the liquid and it occurs under the liquid's free surface. When the high laser power light is focused on a small spot of the liquid trough appropriate optic so called optical breakdown of the liquid occurs producing a shock wave followed by a single bubble. This type of cavitation is called the optical cavitation.

Another way of bubbles formation is through the elementary particles, such as protons and neutrinos, as the particles pass the liquid from an ionization trail for a fraction. These ions transfer energy into electrons, which give up about 1000 eV of energy in a small volume to make rapid local heating. This is generally known as particle cavitation. Hydrodynamic and acoustic cavitation are the product of the tensions liquid rupture under pressure decrease, while the optic and particle cavitation are the result of local deposition of energy [6].

1.1.3 Effects of Cavitation

The cavitation presence in hydraulic machines causes a decrease in the performance but also the mechanical damage of the surface, noise, and vibration. When the cavitation bubbles and bubble structures occur in guide vane blades or in the turbine propeller the effective cross-section of the channel is reduced. This consequently reduces the discharge and the power of the turbine. Turbine efficiency can be reduced by 10% to 20% when the cavitation occurs [7]. Collapsing bubbles or the bubble structures close to the surfaces can lead to surface erosion. As the surface becomes rougher due to the erosion, it increases turbulence and creates crevices or pits that act as nucleation sites for cavitation to occur. Moreover, cavitation has also become a concern in the sustainable power source division because it might happen on the blade surface of the tidal stream turbine [7]. Cavitation is an essential limiting factor in the design of many hydraulic machines as pumps, turbines, hydraulic systems and others.

Figure 1.2: Major cavitation damage to the blades at the discharge from a Francis turbine [35].

Apart from negative effects, cavitation also has a positive effect in many applications. In the field of medicine, the cavitation bubble cluster has been used to break kidney stones in shock wave lithotripsy [8]. Besides, cavitation bubbles may be able to manipulate the DNA in individual cells, creating minute incisions or target cancer cells [9]. Additionally, food and beverage industries use the principle of hydrodynamic cavitation as an effective tool to homogenize, pasteurize, break, or mix food macromolecules [10]. Cavitation is also an effective technique that can be used in wastewater treatment. Hydrodynamic cavitation, which is created using a single hole orifice, is combined with different chemical oxidants for degradation of dye wastewaters [11].

1.1.4 Dynamics of Cavitation Bubble

The cavitation field is composed from individual bubbles that create structures. To understand the behavior of the cavitation it is necessary to understand first the behavior of the individual bubbles. First studies focused on liquid motion around a spherical cavity within an infinite constant pressure field of liquid were conducted by Besant [2]. Later work by Rayleigh [2] was focused on the behavior of the spherical cavity in liquid. Rayleigh also described the pressure field around the bubble during the implosion leading to the pressure concentration and reformulated possible reason of the cavitation erosion. The Rayleigh model was later extended by Plesset [2] to vicious and non-compressible liquids.

The most common model to describe the spherical bubble dynamic in incompressible viscous liquid is so called *Rayleigh-Plesset* equation which has the following form

$$\rho\left[R\ddot{R}+\frac{3}{2}\dot{R}^2\right]=P_V-P_\infty(t)+P_{g0}\left(\frac{R_0}{R}\right)^{3\gamma}-\frac{2S}{R}-4\mu\frac{\dot{R}}{R} \qquad (1)$$

where μ is the liquid viscosity, S the surface tension, ρ the density of liquid, P_V the pressure of vapor inside the bubbles, R_0 the initial bubble radius, $\dot{R}$ and $\ddot{R}$ are the first and second order derivatives of bubble radius with respect to time, γ the polytropic exponent of the gas, $P_\infty(t)$ the pressure far distance form bubble, P_{g0} the pressure of gas inside the bubble at initial state. The simple considerations based on this equation can be used to describe some stages during the bubble live period. If the viscosity and surface tension effects are neglected a formula indicating the bubble wall velocity during the collapse can be formulated in the form

$$\dot{R}\cong-\sqrt{\frac{2}{3}\frac{P_\infty-P_V}{\rho}\left[\left(\frac{R_0}{R}\right)^3-1\right]} \qquad (2)$$

This equation shows that the bubble wall velocity in the final stages of the implosion is very high as the bubble radius tends to zero. When the radius (R) is considered zero, also the bubble collapse time can be estimated. This collapse time is known as the Rayleigh time τ [12]:

$$\tau\cong 0.915R_0\sqrt{\frac{\rho}{P_\infty-P_V}} \qquad (3)$$

Note that this collapse time correlates very accurately with experimental measurements.

1.1.5 Bubble collapse

The cavitation effect resulting in the cavitation erosion are mostly connected to the cavitation bubble collapse. During the bubble collapse the pressures and temperatures reach very high magnitudes resulting in shock wave generation and bubble shape deformation. When the bubble is located close to the surface the bubble shape is deformed creating a liquid jet towards the wall. All these effects are the sources of the cavitation erosion. To be able to measure the magnitude of the interaction between the bubble and the wall it is appropriate to introduce some sensor. The production of such a sensor is the goal of this thesis.

1.2 Objective

The purpose of this work is to manufacture sensors that can be applied to the measurement of the cavitation bubble wall interaction for a single bubble or for a cavitation field. The study is focused on comparing different sizes of the active area of the sensors and also to compare the produced sensors with commercially available sensors. For this propose the individual step for the thesis were formulated as follows:

- A study of methods for making of piezoelectric sensors for the cavitation impact measurements with a particular focus on thin-film sensors.
- Basic properties of piezoelectric film sensors towards the cavitation impact measurement.
- The explanation of a methodology for the fabrication of piezoelectric sensors for the cavitation impact measurement.
- Design and creation of piezoelectric film sensors of different sizes and setup for the cavitation impact measurement.
- The testing of an appropriate cover for the sensor protection.
- The calibration of the sensors using the ball drop method.
- Testing sensors with acoustic cavitation.

2 LITERATURE REVIEW

This chapter presents the fundamental properties of the piezoelectric thin-film sensor towards the cavitation impact measurement and, review of the method used for the fabrication of the piezoelectric film sensors.

2.1 Piezoelectric Film Sensors

In 1969, Kawai found a high piezoelectric property in the polarized fluoropolymer, polyvinylidene fluoride (PVDF) [13]. The polymerization of vinylidene difluoride produces polyvinylidene fluoride. It has a glass transition temperature (Tg) around −35 °C and is normally 50-60 % crystalline [14]. It is produced such as sheet, tubing, films, plate, piping products and an insulator for premium wire. Piezoelectric PVDF film is an anisotropic material since its mechanical responses, and electrical output depends on the axis of the applied mechanical stress or electrical field. Axes are noted 1, 2, and 3 representing stretch direction, transverse direction, and thickness direction, respectively [15]. Piezoelectric film is a flexible lightweight film with excellent sensitivity, low density, wide frequency response, low acoustic impedance, high elastic compliance, high voltage output (10 times higher than piezoelectric ceramics when the same force was applied) and other outstanding mechanical properties [16]. The Piezoelectric film material is also very stable (resisting moisture and most chemical). After the development of several years, PVDF piezoelectric film has become a type of piezoelectric sensing material with excellent performance. The PVDF sensor is fabricated based on the piezoelectric film, which is capable of generating an electric charge when applied to mechanical stress [17]. Table (1), illustrates the basic parameters of the polyvinylidene fluoride (PVDF) material.

The voltage may be detected on the lower and upper side of the piezoelectric film. The voltage will disappear when stress is removed, called a direct piezoelectric effect. Oppositely, the mechanical strain that comes from the internal of the piezoelectric material resulting from an applied electrical field is called the reverse piezoelectric effect. The Sensor has been used to manufacture sensors and actuators for many applications such as shock impact and pressure sensors, biomedical, acoustic, tactile sensors, active vibration control, and structural health monitoring of civil and aerospace structures. PVDF film is beneficial for sensing applications and it is rarely used as an actuator when applications require the transmission of high magnitudes of force.

Table 1: Basic parametrs of polyvinylidene fluoride (PVDF) material [16].

Symbol	Parameter	Value	Units
t	Thickness	2, 28, 52, 110	μm
d_{31}	Piezo Strain Constant	23×10^{-12}	$\frac{m/m}{V/m}$
d_{33}		-33×10^{-12}	$\frac{m/m}{V/m}$
g_{31}	Piezo Stress Constant	216×10^{-3}	$\frac{V/m}{N/m^2}$
g_{33}		-330×10^{-3}	$\frac{V/m}{N/m^2}$
C	Capacitance	380 for 28 μm	pF/cm^2 @ 1KHz
$\varepsilon/\varepsilon_0$	Relative Permittivity	12-13	-
ρ_m	Mass Density	1780	kg/m^3
ρ_e	Volume Resistivity	$> 10^{13}$	Ohm meters
$tan\ \delta_e$	Loss Tangent	0.02	@ 1kHz
Y	Young's Modulus	2-4	$10^9\ N/m^2$
P	Pyroelectric Coefficient	30×10^{-6}	$C/m^2\ K$
-	Temperature Range	-40 to 80…100	°C
-	Water Absorption	<0.02	% H_2O
-	Maximum Operating Voltage	30	V/μm, DC, @25°C
-	Breakdown Voltage	80	V/μm, DC, @25°C

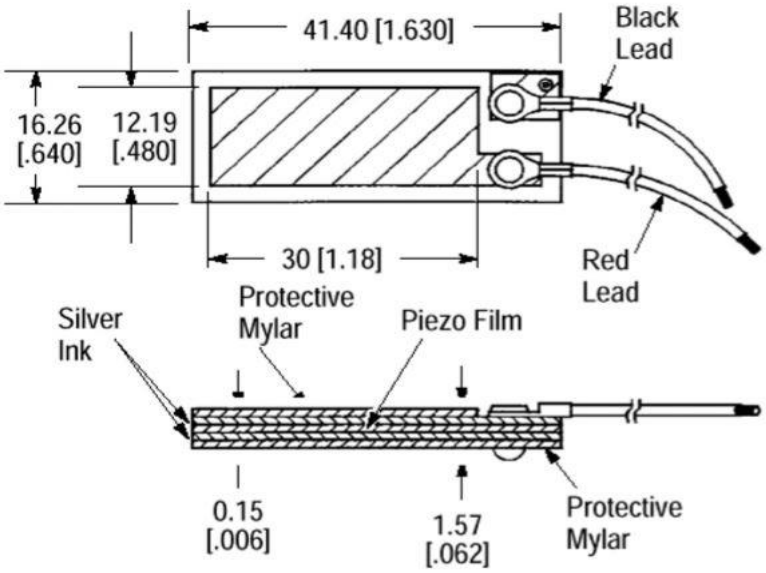

Figure 2.1: Schematic cross-section of a PVDF sensor [32].

The schematic cross-section and photograph of the produced PVDF sensor LDT1-028K/L, by Measurement Specialties Inc. (MSI) is shown in Figure 2.1 and Figure 2.2, respectively. PVDF sensor consists of five layers: two protective Mylar layers, two silver ink layers, 28μm thick PIEZO film and total thickness 40 μm. It has a high sensitivity of 0.013 V/N given by manufacturer [18]. Dual wire leads attach to the sensor for voltage output. It has a capacitance of 1.38 nF.

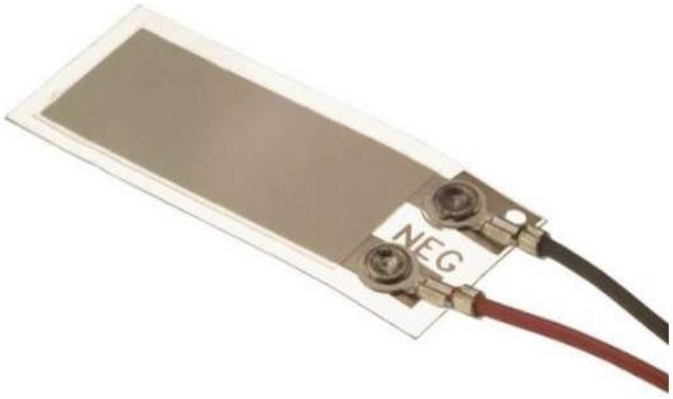

Figure 2.2: Photograph of the PVDF sensor (LDT1-028K) [32].

2.2 Properties of Piezoelectric Sensors

2.2.1 Linear constitutive piezoelectric sensors

PDVF sensor is a piezoelectric plastic material that produces electric field on both sides of the film when it is mechanically deformed [19]. Figure 2.3 show a schematic of PVDF film.

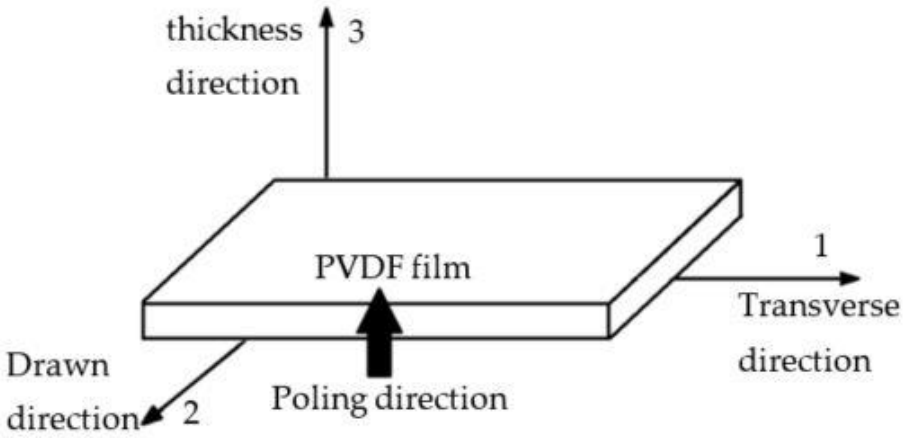

Figure 2.3: Schematic of PVDF film [19].

The linear constitutive piezoelectric equations are:

$$S_{ij} = s^{E}_{ijkl} T_{kl} + d_{kij} E_k \quad (4)$$

$$D_i = d_{ikl} T_{kl} + \varepsilon^{T}_{ik} E_k \quad (5)$$

Where *S* is the strain component, s is elastic compliance constants, *T* is the mechanical stress, *d* is the piezoelectric strain constants, *E* is the electric field component, *D* is the electric displacement, ε is the dielectric permittivity and *i*, *j*, *k*, and *l* are the values 1, 2, 3 and are tensor notations. Both equations (4) and (5) are tensor equations. Strain, stress and elastic compliance constant are second order tensor, piezoelectric strain constants are third order tensor, and the fourth order tensor is elastic compliance constants.

A single subscript may simplify equation (4) and (5) with compressed matrix notations:

$$S_p = s^{E}_{pq} T_q + d_{kp} E_k \quad (6)$$

$$D_i = d_{iq} T_q + \varepsilon^{T}_{ik} E_k \quad (7)$$

Table 2 shows the relation between the compressed matrix and the tensor notations.

Table 2: Tensor and matrix notations.

Tensor notation (ij or kl)	Matrix notation
11	1
22	2
33	3
23 or 32	4
31 or 13	5
12 or 21	6

When the objective of the PVDF film is to be used as a sensor, there is no external field in the film. Therefore, the electric field E equal zero, the equation (7) can be written as:

$$D_i = d_{iq} T_q \tag{8}$$

which equation (8) can be expanded as:

$$\begin{bmatrix} D_1 \\ D_2 \\ D_3 \end{bmatrix} = \begin{bmatrix} 0 & 0 & 0 & 0 & d_{15} & 0 \\ 0 & 0 & 0 & d_{24} & 0 & 0 \\ d_{31} & d_{32} & d_{33} & 0 & 0 & 0 \end{bmatrix} \begin{bmatrix} T_1 \\ T_2 \\ T_3 \\ T_4 \\ T_5 \\ T_6 \end{bmatrix} \tag{9}$$

Where D_1, D_2 and D_3, the electric displacements are in the 1, 2 and 3 directions, the piezoelectric strain constants d_{31}, d_{32}, d_{33} are in the 1, 2 and 3 directions, the piezoelectric shear strain constants d_{24}, d_{15} are in directions 1 and 2, the mechanical stress T_1, T_2, T_3 are in the 1, 2 and 3 directions and T_4, T_5, T_6 are the shear stress in direction 1, 2 and 3 [19].

The electric displacement D is related to the charge generated by the relation [20] [21]:

$$q = \iint [D_1 \quad D_2 \quad D_3] \begin{bmatrix} dA_1 \\ dA_2 \\ dA_3 \end{bmatrix} \tag{10}$$

Where dA_1, dA_2, and dA_3 are the components of the electrode surface in the 2-3, 1-3, and 1-2, respectively, and the charge generated q depends on the element of electric displacement D and the electrode area dA.

2.2.2 PVDF Sensors Operation Modes

The PVDF sensor as the force sensor or pressure sensor can be used in two different modes: the d_{31} mode and the d_{33} mode. The mode of operation shown in figure 2.4.

The stress or force is applied to the upper or lower surface of a sensor along the 3-direction of the sensor called the 33-mode operation. The sensor must be put in the right position, so that it can be fall directly in the path of the applied load.

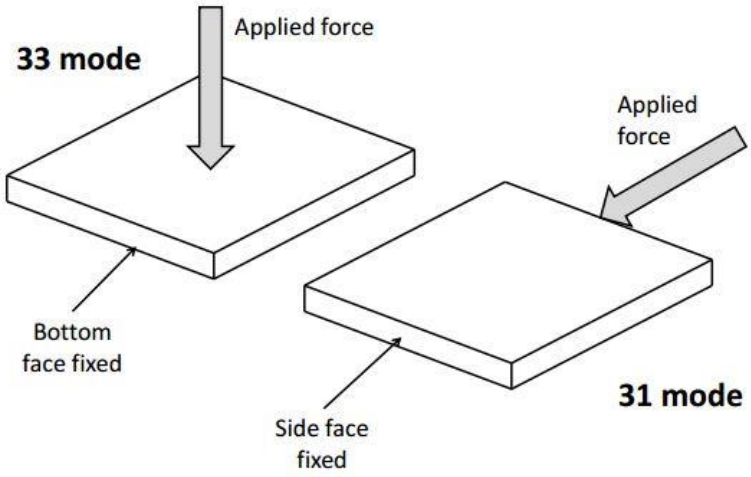

Figure 2.4: 33 mode of operation (left), 31 mode of operation (right) [29].

In the 31-mode of operation, the force is applied in the longitudinal or along the 1 direction. This operation mode can be achieved by direct stretching the piezoelectric element by bonding it to a substructure that undergoes bending. Hu et al. [19] designed a PVDF sensor to detect wrist motion signals based on 31 operation mode. Based on the value of strain and stress constant in table 1, it seems that energy generated in the 31-mode is better than 33-mode. The mode of operation is shown in Figure 2.4.

2.2.3 Source capacitance

Capacitance is the ability of an object to the store electric charge when two parallel conductive surfaces are prevented by an insulating material like air, rubber, or paper called the dielectric. In a PVDF sensor, the conductive electrodes printed on each surface of the foil are the capacitance plates. The capacitance of the sensor depends on the plate area. Large surface of the film will have a larger capacitance than the small surface at the same

thickness. When the thickness of the film decreases, the capacitance increases at the same size.

The capacitance can be expressed as:

$$C_s = \varepsilon \frac{A}{t} \tag{11}$$

Where C_s is the capacitance of the PVDF film, t is the thickness of film, A is the area of film printed by electrodes and ε is the permittivity which is

$$\varepsilon = \varepsilon_r \varepsilon_0 \tag{12}$$

Where ε_0 the permittivity of free space constant, 8.854 x 10^{-12} F/m and ε_r the relative permittivity equal 12 for PVDF.

2.2.4 Equivalent circuit of PVDF Film

PVDF sensor is a type of capacitive sensor. The equivalent circuit models of the PVDF sensor have two models. The first one is used as a voltage source in series with a capacitance of the PVDF sensor and another is used as an internal resistance in parallel with a capacitance of the PVDF film called as a charge source. Figure 2.5(a) illustrates the voltage source where V_t is the open-circuit voltage of the sensor, and V_s is the voltage generated

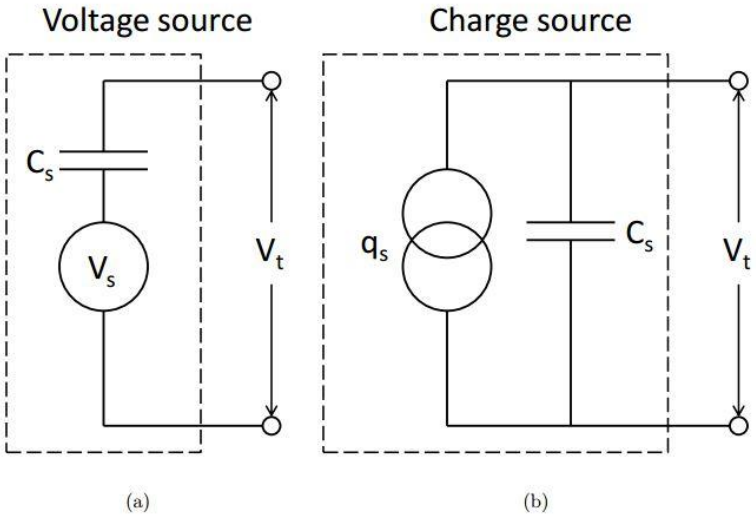

Figure 2.5: Type of electric model of the PVDF film (a) the Voltage source and (b) the Charge source [29].

by the piezoelectric film (directly proportional to the applied force), and C_s the internal capacitance of the PVDF sensor. The voltage source equivalent circuit of the sensor is most commonly used for many applications; however, it has limit value for very high frequencies

like used in ultrasound transducers. Figure 2.5(b) shows the charge generator. The dashed rectangle in both pictures represent the components of PVDF film.

The open-circuit voltage of the sensor can be calculated as [22]:

$$V_t = \frac{Q}{C_s} \tag{13}$$

where V_t is the open-circuit voltage, Q is the electrical charge developed on film and C_s is the film capacitance.

2.2.5 Temperature Effect of PVDF film

Many of the piezoelectric sensitivity of PVDF film is dependent on temperature between the glass transition temperature (-40°C) and the breakdown of the piezoelectric film (80°C); the magnitude of the sensitivity increases with temperature [23]. Figure 2.6 shows that piezoelectric constant d_{33} and g_{31} increase with temperature.

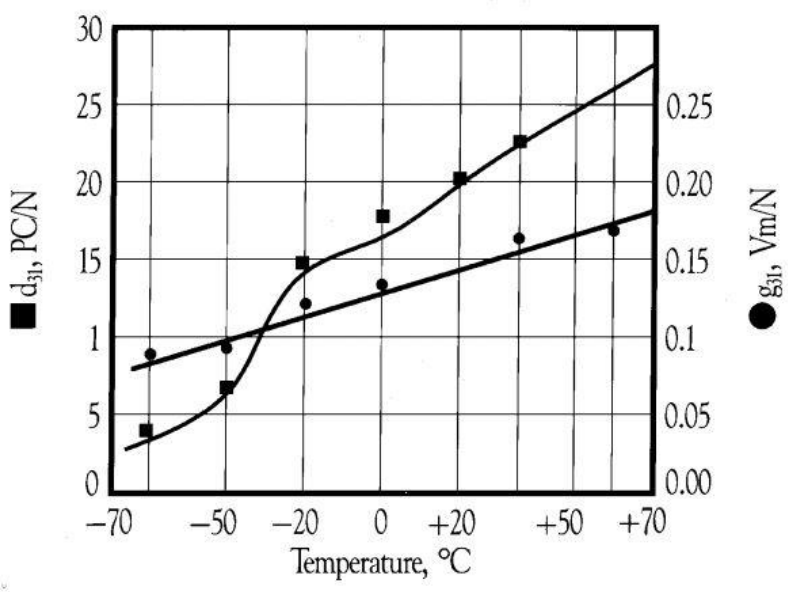

Figure 2.6: Temperature coefficient for d33 and g31 constants of PVDF [16].

2.3 Production of Piezoelectric Film Sensors

2.3.1 Jiqing et al., 2019 [17]

Jiqing et al. fabricated a PVDF sensor for the measure of the dynamic pressure field of the blade tip in an axial flow compressor. The PVDF sensor was fabricated based on its

piezoelectric polyvinylidene fluoride (PVDF) polymer. The sensor was tested with the pressure up to 3.5 KPa, and the sampling frequency is 20 kHz. From this study, the PVDF film sensor was made up of a 30 μm thick PVDF film with aluminum electrodes, two shielding layers, and two protective layers. Figure 2.7 shows the cross-sectional view of the PVDF sensor. The PVDF film material is manufactured by Jinzhou Kexin Electronic Material Co., Ltd. (Liaoning, China). With this PVDF material, the sensor can measure pressure up to 20 GPa and frequency up to 10^8 Hz. The basic properties of the material are shown in Table 4. The sensitive area of the sensor is 3 mm × 3 mm, which is overlapped by positive and negative electrodes in Figure 2.8.

Table 3: Basic properties of PVDF material.

Items	Value	units
Piezo Strain Constant d_{33}	pC/N	21
Piezo Voltage Constant g_{33}	V.m/N	0.2
Frequency Response	Hz	$10^{-2}$to 10^8
Pressure Range	GPa	0 to 20
Acoustic Impedance	Pa. s/m^3	$2.5 - 3 \times 10^5$
Yield Strength	N/m^2	$4.5 - 5 \times 10^6$
Density	kg/m^3	1780
Poisson's Ratio	-	0.3
Operating Temperature Range	°C	-40 to 80
Thickness	μm	30

A protective layer or insulating layer at the top and the bottom sensor is produced by PET plastic film to protect the body of the sensor from erosion or wear. Below the protective layer is a shielding layer to protect the sensor from the noise that comes from the test site and electromagnetic interference. This layer is made of aluminum. The extraction electrodes are a positive electrode and a negative electrode. Both of them are made of aluminum, and the middle is a PVDF film. The shielding layer and the extraction electrodes are connected by insulation adhesive.

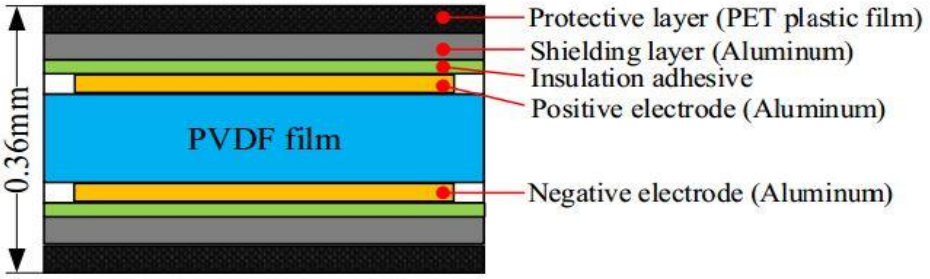

Figure 2.7: Cross-sectional view of the PVDF sensor [17].

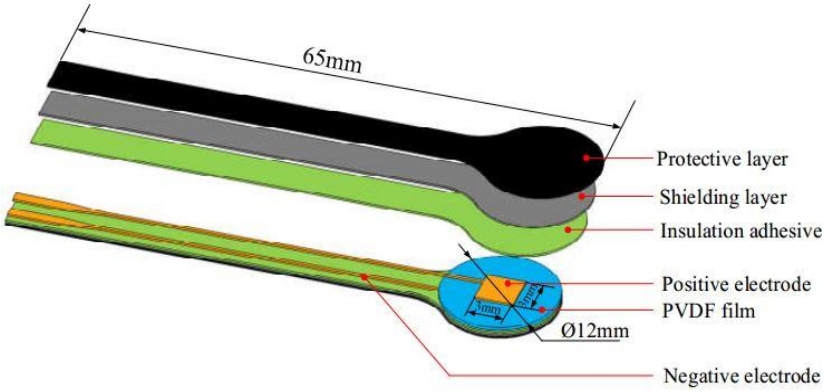

Figure 2.8: Expanded view of the PVDF sensor [17].

The electrode on the PVDF film, which is the detecting point of the sensor, are produced by the photolithography process with the pattern of positive and negative electrodes, and the thickness is 1.5 μm (lithography equipment, SSB260/20T, Shanghai Micro Electronics Equipment Co., Ltd, Shanghai, China). After bonded together, the shape of the sensor is cut by the laser. The final thickness of the sensor is 0.36mm. The top view of sensor shown in Figure 2.9.

Figure 2.9: Top view of the PVDF Sensor [17].

2.3.2 Wang et al., 2005 [24]

In the study of Wang et al., a PVDF sensor array was developed for the measurement of the impulsive pressure generated by the cavitation bubble collapse. The reason for application of the PVDF film was high response frequency, good durability, a broad range of linearity, and low acoustic impedance.

The PVDF sensor was produced on a 25 μm thick aluminum metalized polarized PVDF film (FV301926, Goodfellow Cambridge Ltd, UK) by using an excimer laser micro-machining system (PS-2000, Excitech Ltd, Oxford, UK). The laser system KrF with ultraviolet light pulses with energies up to 350 mm is shown in Figure 2.10. The laser beam is focused on the surface of the film by changed shape and size after passing a mask, using a 10× projection optics. PC-based Programmable x-y-z precision stage with a resolution of 1 μm is used to control the position and path of the laser beam related to the target surface. The maximum laser energy that transports to the target surface can be approximately 2 mJ/cm^2. The smallest dimension of the laser beam that only removes the top electrode of the film and keeps the bottom one intact is 10 μm.

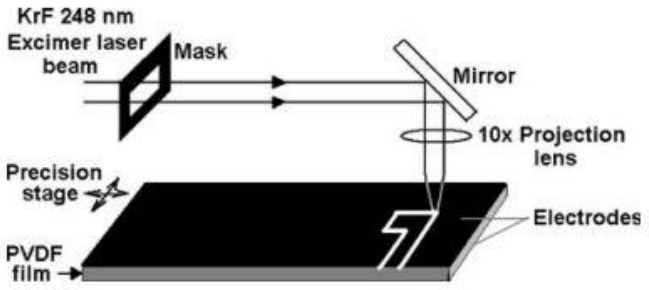

Figure 2.10: Electrode patterning of PVDF film using excimer laser micro-machining [24].

As illustrated in Figure 2.11, the layout of the PVDF sensor array with the four sensing elements is patterned in the same film. The sensitive area of each sensing element is 4.8 mm × 4.8 mm, and the distance between the centers of each element is 6.4 mm.

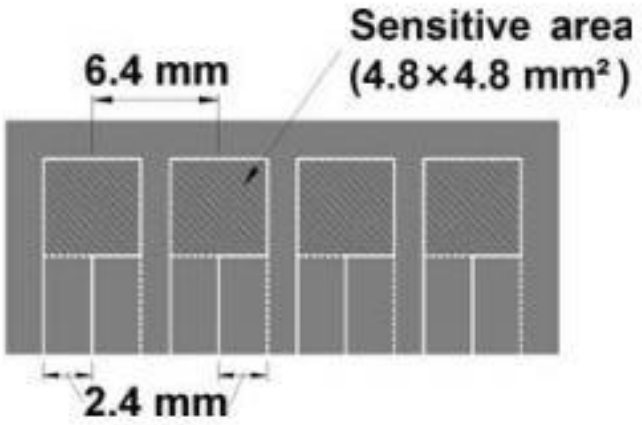

Figure 2.11: Layout of the PVDF array sensor [24].

2.3.3 Gaofeng, et al., 2018 [15]

The aim of the study of Gaofeng, Lui, Li, Cui, Guo, and Shang was to develop a flexible thin-film single-point force sensor based on the piezoelectric of PVDF film. It was possible to dynamically measure a single-point force in the mechanical or biomedical field. For Measurement range of the sensor starts from 0 to 6217 N, and the working temperature is between -40 °C and 80 °C. The dimension of the sensor is 75 mm × 20 mm × 1mm. The structure design is shown in Figure 2.12. The insulative layer was in between two conductive electrodes. To increase the deformation of the PVDF film, the reference space is used. The sensor was fabricated under the following condition: fabrication pressure is 0.975 MPa and working temperature 25 °C. A plastic film was adhered to the surface of each conductive electrode film by using insulative glue. The supporting rack is put in the circle area of the bottom aluminum electrode film. Conductive glue is used to connect the supporting rack and the aluminum electrode film. Then, the top of the supporting rack is coated by conductive glue to adhere to the PVDF film. Finally, a flexible thin-film single point force sensor from PVDF film is fabricated, as shown in Figure 2.13.

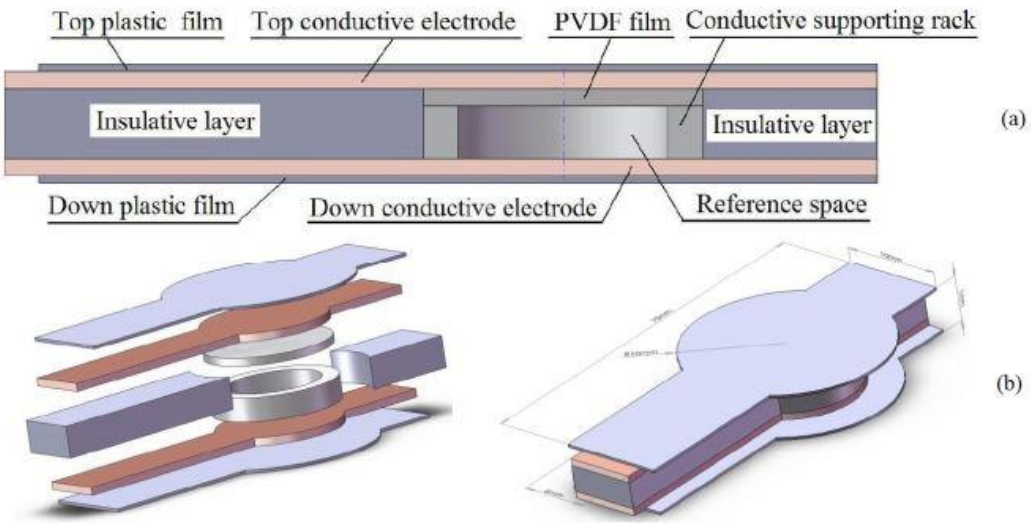

Figure 2.12: Design of single point force PVDF sensor. (a) Cross section drawing of the senor; (b) 3D view and assembly of the sensor [15].

Figure 2.13: Flexible thin-film single point force sensor from PVDF film [15].

3 METHODOLOGY

This chapter describes in details the method of producing PVDF sensors of different sizes, the process for calibration of the sensor, and experiment setup for the ball drop calibration method.

3.1 Sensor Fabrication

3.1.1 PVDF Film Material

The sensor material, PVDF film, produced by TE connectivity Ltd was used to fabricate senor. The film thickness was 28 μm with 800 Å electrode Cu-Ni metallization, consisting of a 700 Å copper layer and a 100 Å nickel layer. It has a capacitance of 1.38 nF. The full size of the sheet is 8" × 11". The typical specifications of the film are listed in Table 4. The Metallized piezo film sheets are shown in Figure 3.1.

Table 4: Specifications of the film.

Electro-Mechanical Conversion	(1 direction) 23 x 10-12m/V, 700 x 10-6N/V (3 direction) -33 x 10-12m/V
Mechano-Electrical Conversion	(1 direction) 12 mV per micro strain, 400mV/μm, 14.4V/N
Pyro-Electrical Conversion	(3 direction) 13 mV/N
Capacitance	1.36 nF
Maximum Operating Voltage	DC: 280 V (yields 7 μm displacement in 1 direction)
Maximum Applied Force (at break, 1 direction)	6-9 kgF (yields voltage output of 830 to 1275 V)

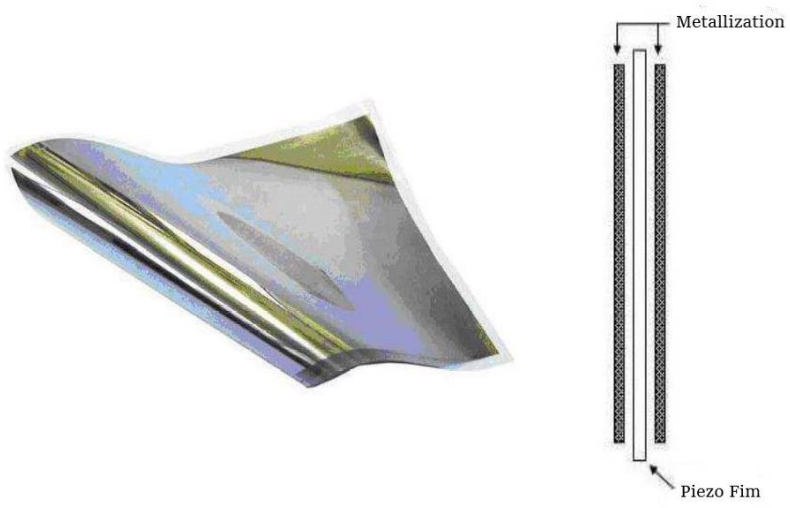

Figure 3.1: Metallized piezo film sheets [34].

3.1.2 Protective Material (Kapton Tape)

The top and bottom layers are known as protective layers or insulating layers that are used to avoid wear or corrosion on the surface of the PVDF film. Kapton Tape 65 μm is used as a protective layer of this sensor, designated by EUROSTAT. Kapton tape specifications are shown in Table 5.

Table 5: Kapton tape sepcifications

Material	Low static polyimide (Kapton) with silicone adhesive.
Thickness	65 μm
Width	12.7 mm
Elongation	63%
Tensile strength	5kg/f/c (ASTM D3759)
Chemical resistance	Good (test at 180 °C/hour in heating oven).
Operation temperature	260 °C
Lowest temperature of use	10 °C
Static Charges	< 50 Volts (@ 50% RH, 20 °C

3.1.3 PVDF Sensor Fabricated by Photolithography Technique

The patterns of positive and negative electrodes of the film are fabricated by photolithography. Photolithography is a chemical process in which an image is transferred onto a substrate. It is useful to create a sensor with a small size, shape, or a matrix of sensors in a few nanometers. A general flow chart of the photolithography process can be seen in Figure 3.2.

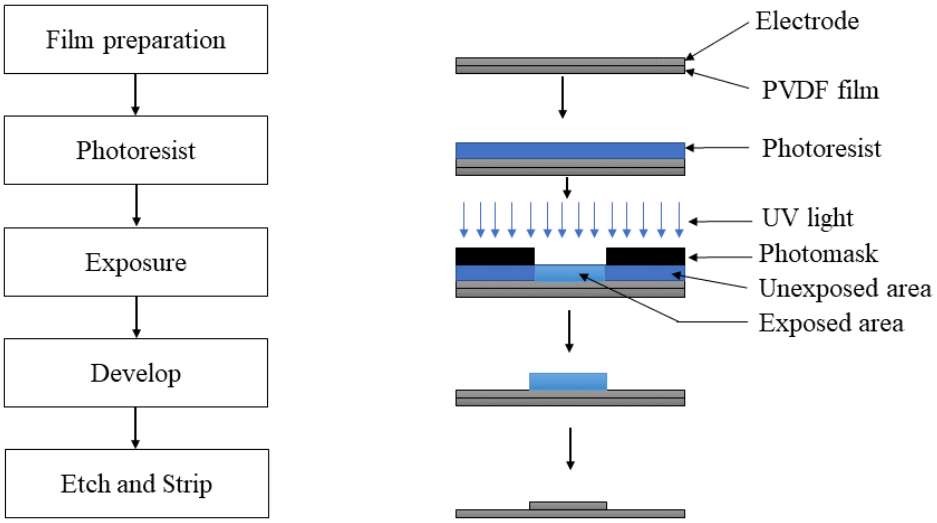

Figure 3.2: Figure Flowchart of the photolithographic process.

3.1.3.1 Film Preparation

The first step of the photolithography process is the preparation of PVDF film, which aims to improve the photoresist's adhesion to the film. It is done by cleaning to remove any contamination.

3.1.3.2 Photoresist

The photosensitive film is used as a negative photoresist. The film has a protective layer on both sides and the resist layer in the middle, which the 50 mm thickness. The photosensitive film is stuck to a PVDF film by electrically heated lamination rollers (REMA Laminator, RLM 419P) under the temperature 110 °C. In this process, the soft protective layer inside of photosensitive film is removed. REMA Laminator, RLM 419P is shown in Figure 3.3.

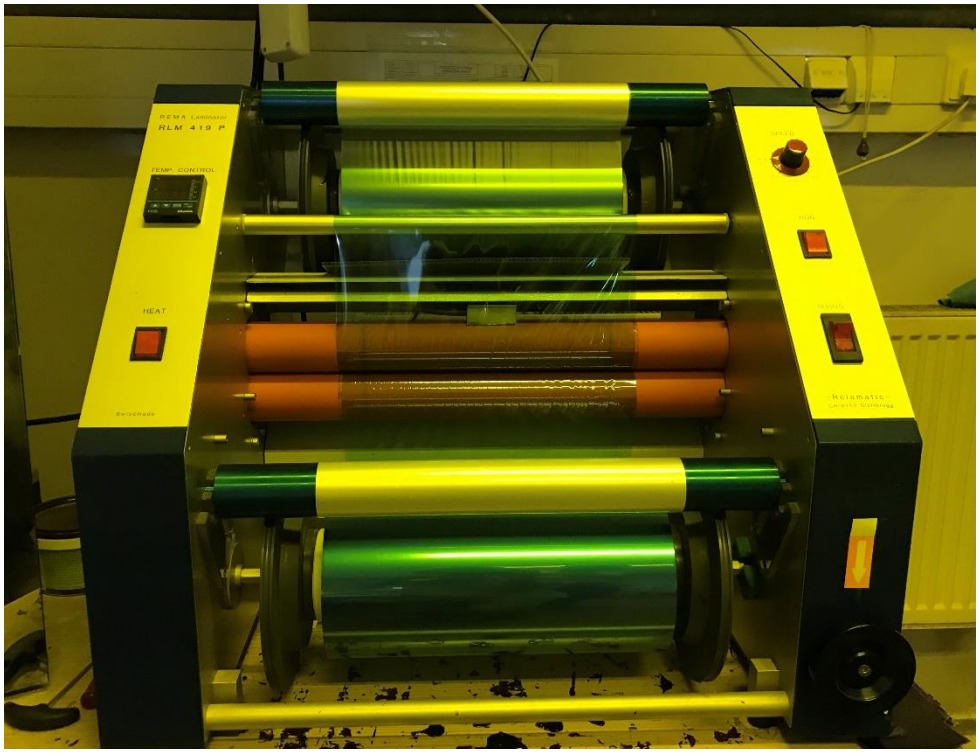

Figure 3.3: REMA Laminator, RLM 419P.

3.1.3.3 Exposure

A photomask was created by printing on plastic foil or glass plate while its geometry was drawn in CAD software. Subsequently, the film was put in between two photomasks. Then, UV light was applied on the photoresist for 80 seconds through a photomask by Hellas Exposure Unit BUNGARD (see Figure 3.4). The resist was exposed and undergone chemical reactions that made differences between exposed and unexposed parts of the photoresist.

Figure 3.4: Hellas Exposure Unit BUNGARD.

3.1.3.4 Development

Once exposed, the photomask and second protective layer on the top of photosensitive film were removed. The photoresist was developed with sodium carbonate solution (Na_2CO_3) by spraying for 150 seconds. Then, the resist that did not expose to UV light was removed.

3.1.3.5 Etch and strip

The etching removed the electrodes that were not covered up with photoresist by using Ferric chloride solution ($FeCl_3$) in 10 seconds. After finished the etches, the remaining photoresist is removed with Sodium hydroxide (NaOH). Figure 3.5 is the PVDF film before and after the Photolithography process.

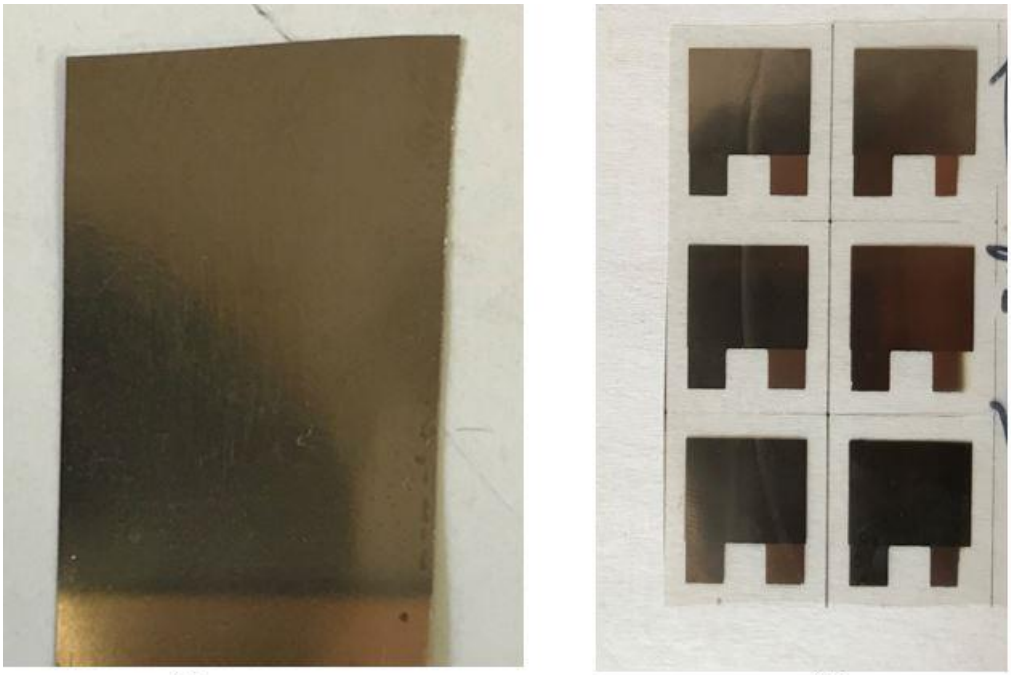

Figure 3.5: PVDF foil before (a) and after (b) Photolithography process.

3.1.4 Leads attachment of Sensor

Leads attachment is accomplished by using two copper rivets to affix to the offset conductive traces on the PVDF film. This method is easy to apply and durable enough to meet the operating requirements of the sensor. To implement this leads attachment technique, the first thing to do is to punch a hole with a diameter of 1 mm into PVDF foil on the metallization outlets. Then, a ring made of brass sheet and plastic foil with a hole of 1 mm inner diameter is prepared by cutting. The next step is to connect the wire with the rivet. Last step is to place the plastic ring into the rivets and mechanically press the rivets to make reliable interconnection (Figure 3.6).

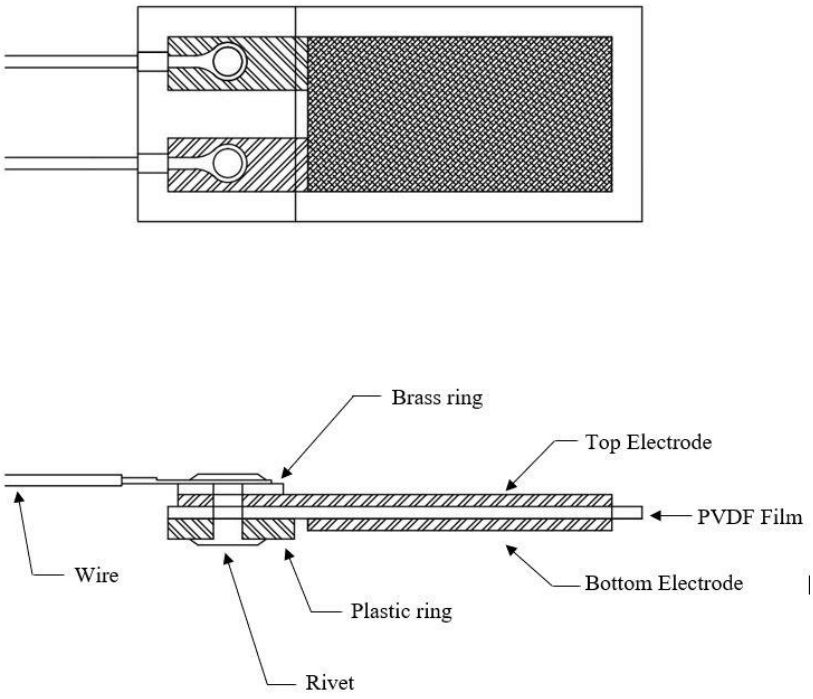

Figure 3.6: PVDF film connected with rivets.

3.1.5 Sensor Synthesis

After the competed process mentioned above, the sensor is composed of a 28 μm thick PVDF foil with a Cu-Ni electrode and two protective layers on both sides, in which the total thickness of the sensor is 158 μm. The sensor has a length of 20 mm and width 15 mm, and the sensitive area is 12 mm × 11 mm, where the area of the electrode. The top and bottom layers of the sensor are protective layers (Kaption tape), and the PVDF film is sandwiched between positive and negative electrodes. A cross-sectional view of the sensor and Photograph are shown in Figure 3.7 and Figure 3.8, respectively.

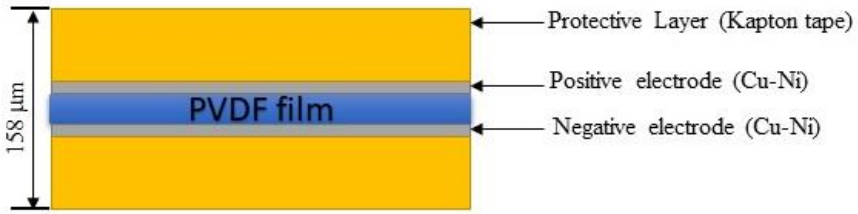

Figure 3.7: Cross-sectional view of the PVDF sensor.

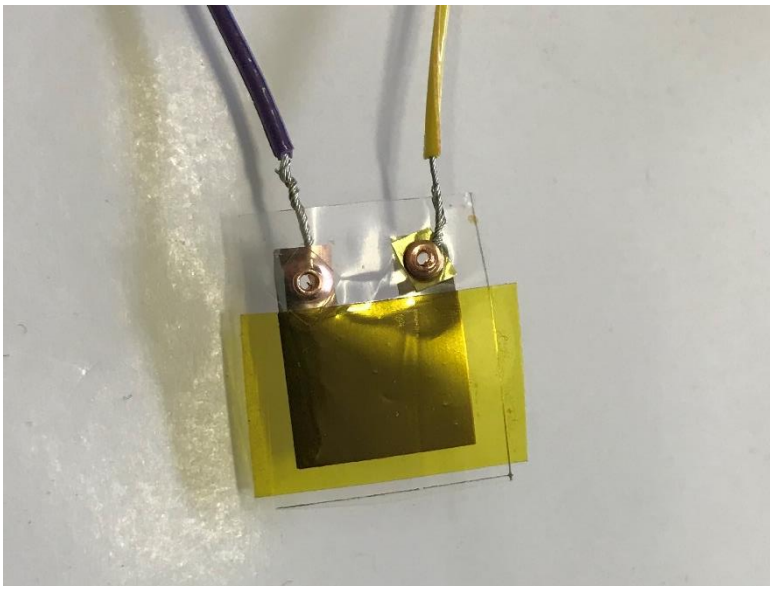

Figure 3.8: Photograph of the PVDF sensor (active area 12 mm x 10 mm).

Three sizes of PVDF sensors are fabricated. Dimensions of PVDF sensors are listed in Table 6.

Table 6: Dimensions of TUL PVDF sensors.

Types of PVDF sensor	Active area dimensions
PVDF sensor (12 mm x 30 mm)	12 mm × 30 mm
PVDF sensor (12 mm x 10 mm)	12 mm × 10 mm
PVDF sensor (12 mm x 1 mm)	12 mm × 1 mm

3.2 Calibration – ball drop method

The output signal of the piezoelectric PVDF sensor is a voltage. This voltage is proportional to the force or pressure applied to the sensitive surface of the PVDF sensor [25] [26]. The sensor must be calibrated before using it. The calibration of the PVDF sensor will be executed to convert the voltage to force.

The ball drop test method is the most commonly used for the calibration of this sensor [27]. Figure 3.9 shows the scheme of the ball drop technique. The ball is dropped from the initial position h_1, and rebound to the second position of height h_2.The ball is dropped through the

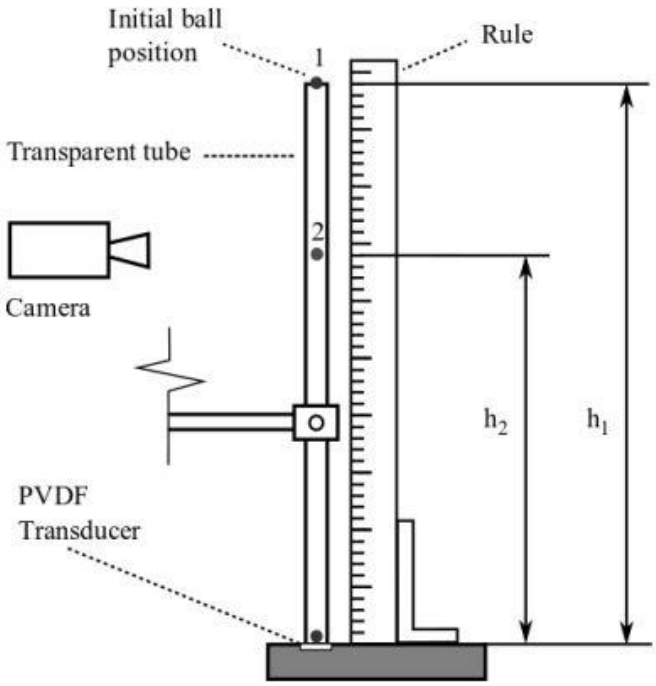

Figure 3.9: Calibration - Ball drop method [25].

glass tube. Height h_1 and height h_2 is measured by line and slow-motion camera because the rebound point h_2 very fast to see the value by the naked eye. During the ball drop, the maximum voltage U_{max} and the time duration of the impact τ are measured by DAQ with Lab view Signal Express software. Calibration signal with a 0.7 g ball and an initial starting position of 400 mm is shown in Figure 3.10.

The mean force can be calculated based on the impulse-momentum theorem [27].

$$F_{mean} = \frac{1}{\tau}\int_{t_2}^{t_1} F(t)dt = \frac{m}{\tau}(v_1 + v_2) \quad (14)$$

Where v_1 is the velocity of the ball at the first point h_1, v_2 is the rebound velocity at point h_2 and $\tau = t_2 - t_1$ is the impact duration time. v_1 and v_2 are calculated from the following formula

$$V_{1,2} = \sqrt{2gh_{1,2}} \quad (15)$$

Where h is the height of the ball, and g is the gravity acceleration. Maximum force can be calculated as

$$F_{max} = 2F_{mean} \quad (16)$$

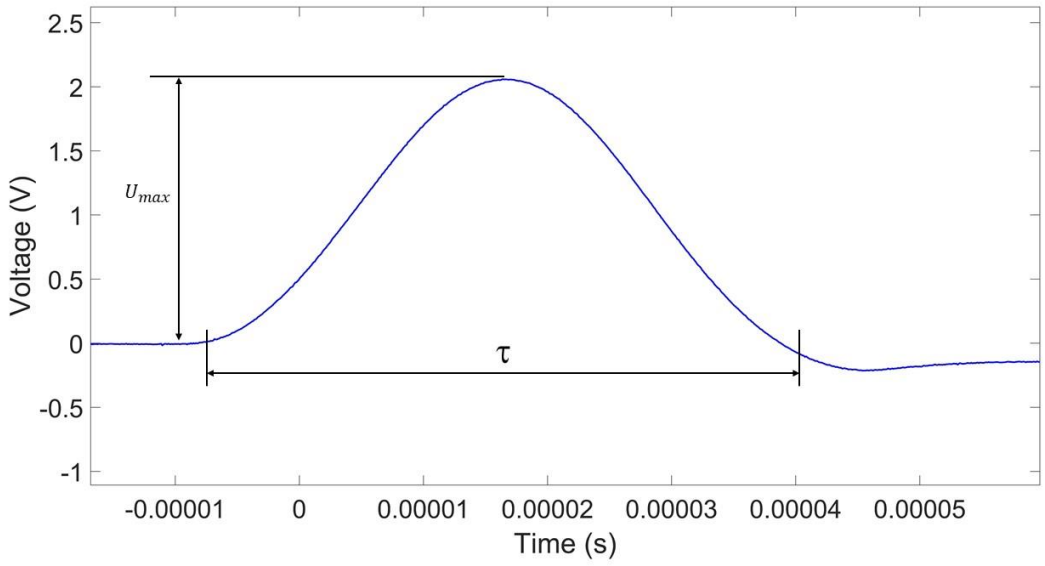

Figure 3.10: Calibration signal with a 0.700 g ball and an initial starting position of 400 mm.

3.3 Experimental Setup

A developed sensor (TUL Laboratory) and the commercial PVDF sensor (DTI-028K/L – Measurement Specialties, Inc.) were chosen to compare. The active part of the film is mounted on a metal plate by using cyanoacrylate glue (Loctite Super Attack Power Flex Gel). The epoxy glue (Bison 5 min) is used to coat the rivet of the sensor for the purpose of preventing a short-circuited by the platform. The surface of the metal plate that contacts with the film must be smooth to avoid having air bubbles when adhering to the film**.** Figure 3.11 shows the PVDF sensor mounted on the metal platform. Dual wire lead attached to the sensor was connected to a DAQ device (Data Acquisition System, the National Instruments - NI PXI-5105 12-bit Digitizer) mounted on the NI PXI-1033 chassis for reading the output signal of the sensor. Then, PXI-1033 is connected to the computer via a PCI card. NI Signal Express software is used to analyze and present data from measurement devices.

Five PVDF film configurations were utilized. The first setup is a PVDF produced by Measurement Specialties, Inc and the second is a developed sensor fabricated by TUL Laboratory in a different size. These PVDF sensors are mounted to a metal plate, as shown in Figure 3.11 to Figure 3.13.

Figure 3.11: (a) MSI PVDF sensor (12 mm × 30 mm), (b) TUL PVDF sensor (12 mm × 30 mm)

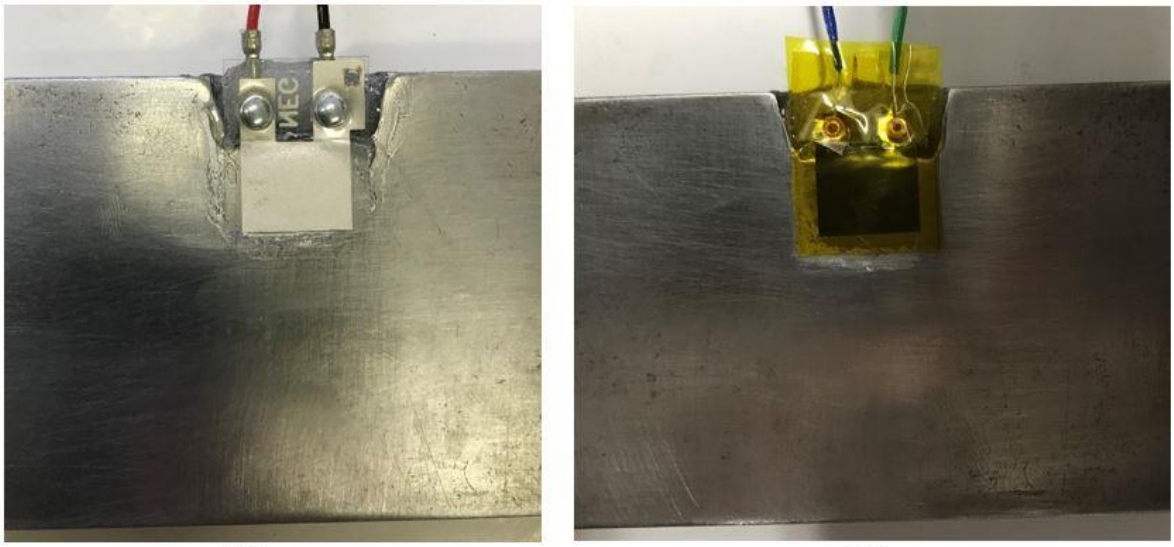

(a) (b)

Figure 3.12: (a) MSI PVDF sensor (12 mm × 10 mm), (b) TUL PVDF sensor (12 mm × 10 mm).

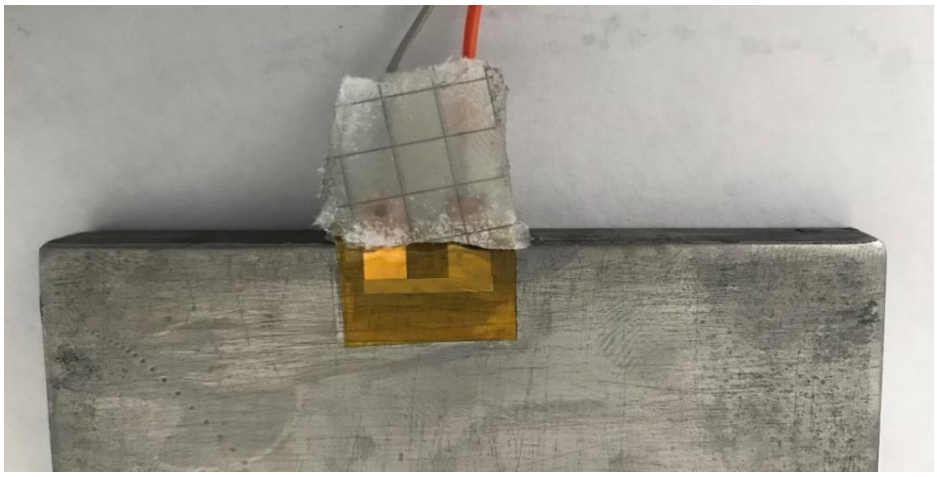

Figure 3.13: TUL PVDF sensor (12 mm × 1 mm).

The guide tube, PVDF sensor, and the data acquisition instrument were installed, as shown in Figure 3.14. In this study, it was decided to use three guide tubes in different lengths 400 mm, 300 mm, 150 mm, and four stainless steel balls of various sizes (0.700 g, 0.441 g, 0.256 g, and 0.132 g). In addition, it was decided to perform five calibration tests for each ball size.

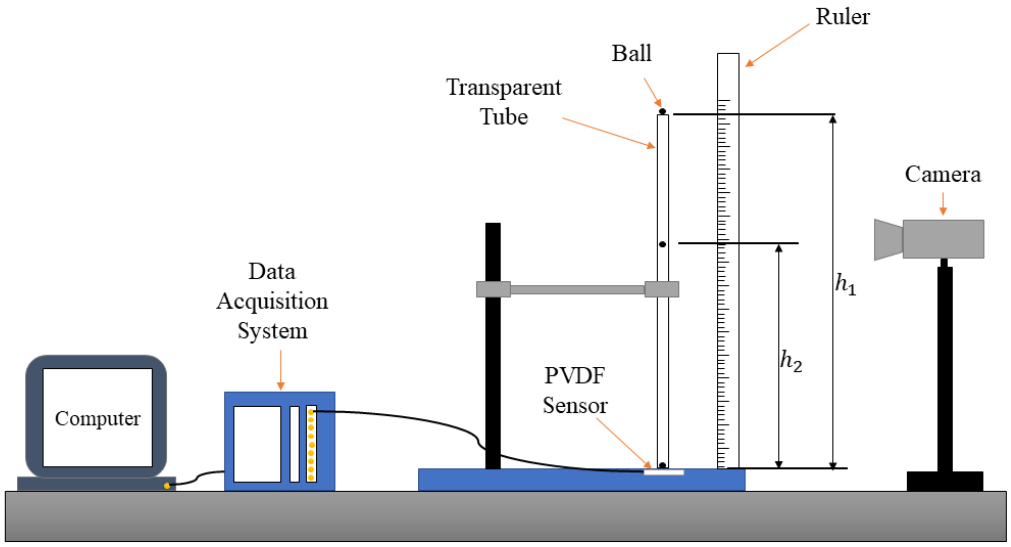

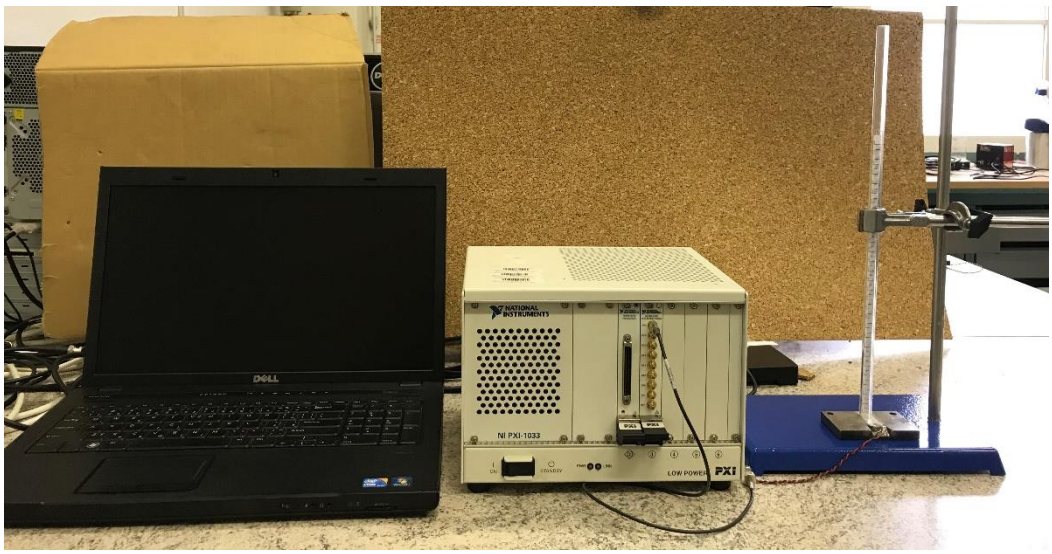

Figure 3.14: Ball drop method calibration PVDF experimental setup.

3.3.1 PVDF Sensor DAQ Setting

The PVDF data are received from the NI PXI505 card to the NI SignalExpress program. One channel of the PXI-505 is connected to the output signal of the PVDF film transducer. The setting used for data acquisition is configured as below:

- Device - PXI 5105
- Channel – 0
- Range - 6 V
- Offset - 0 V
- Probe attenuation – 1
- Coupling – DC
- Input Impedance - 1 Mohm
- Bandwidth - 0 Hz
- Sample Rate (S/s) - 10M
- Record Length – 20000
- Acquire - N Samples

The Trigger tab is set up as such:

- Type – Edge
- Source – Channel 0
- Slope – Positive
- Coupling – DC
- Ref position – 0
- Level (V) – 0
- Max time (s) – 20 s
- Delay (s) – 5m

After complete testing, a signal of the sample can be view at the Display Pane of SignalExpress. Then the data can be export as an Excel file or text file.

3.4 Post-Processing of Signals

The signal of a PVDF sensor is obtained from testing with the three tubes with four ball weights and each ball five trails. This data are rececived from the PVDF film mounted on the metal plate, as shown in Figure 3.12. Figure 3.15 to 3.20 illustrate the signal recorded of the TUL PVDF sensor and MSI PVDF sensor (12 mm × 10 mm) with 400 mm, 300 mm, and 150 mm, respectively. The output signal of the PVDF sensor in the form of the vertical axis is voltage, and the horizontal axis is time. The red, green, blue, and black curves represent the mass balls of 0.132 g, 0.260 g, 0.441 g, and 0.700g, respectively. The graph shows good reproducibility between each ball drop test. This denotes that the voltage generated depends on the length of the tube.

In Figure 3.15, the average maximum voltages were around 2.5 V with the ball of 0.700 g, 1.8 V with the ball of 0.441 g, 1.4 V with the ball of 0.260 g, and 0.8 V with the ball of 0.132 g, when the impact durations were 50 μs, 44 μs, 39 μs, and 35 μs, respectively by the tube 400 mm.

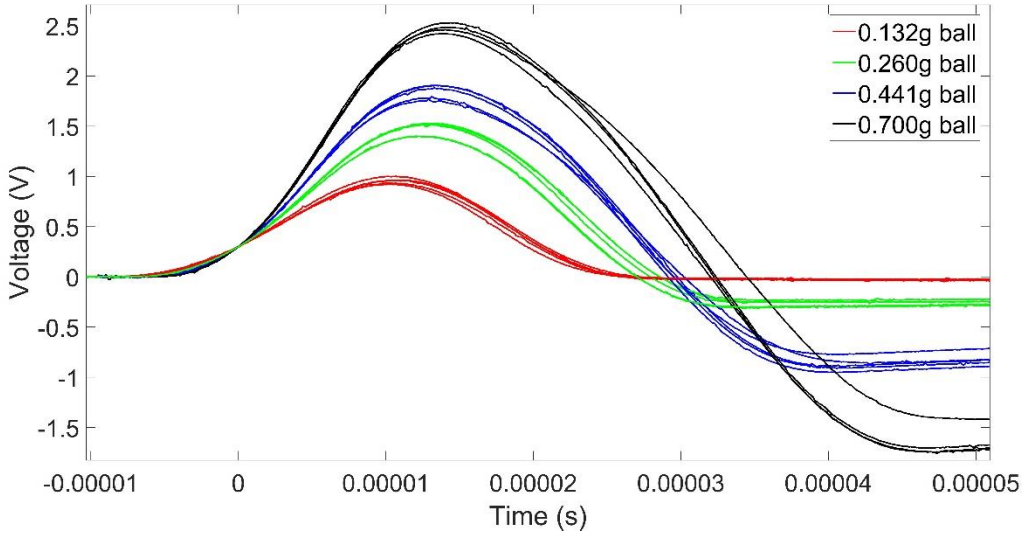

Figure 3.15: Calibration signal TUL PVDF Sensor (tube 400 mm).

In Figure 3.16, the tube's length was reduced to 300mm, so the average maximum voltages also decreased to 2.3 V with the ball of 0.700 g, 1.7 V with the ball of 0.441 g, 1.3 V with the ball of 0.260 g, and 0.7 V with the ball of 0.132 g, while the impact durations were 54 μs, 47 μs, 39 μs, and 37 μs, respectively.

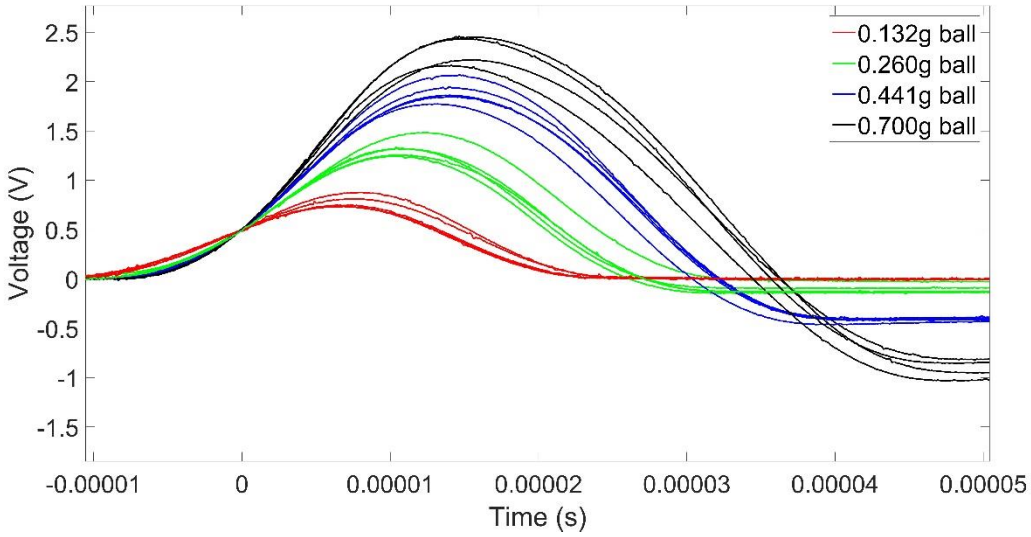

Figure 3.16: Calibration signal TUL PVDF Sensor (tube 300 mm).

In Figure 3.17, the tube for testing was 150 mm. The impact durations were 59 μs, 52.5 μs, 46 μs, 40 μs and the average maximum voltages were 1.65 V with the ball of 0.700 g, 1.2 V with the ball of 0.441 g, 0.77 V with the ball of 0.260 g, and 0.45 V with the ball of 0.132 g, respectively.

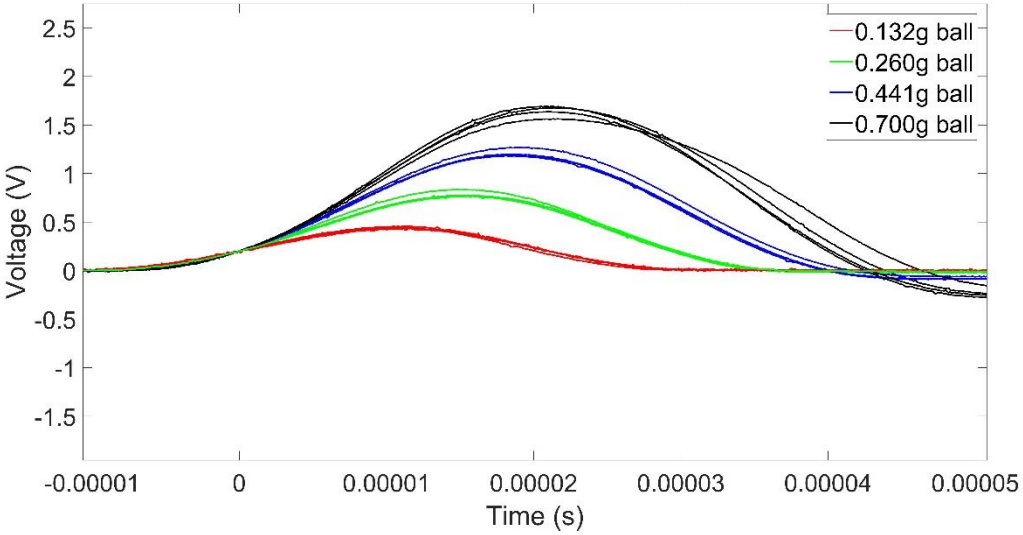

Figure 3.17: Calibration signal TUL PVDF Sensor (tube 150 mm).

In Figure 3.18, the average maximum voltages were around 3.45 V with the ball of 0.700 g, 2.61 V with the ball of 0.441 g, 1.77 V with the ball of 0.260 g, and 1.13 V with the ball of 0.132 g, when the impact durations were 25 μs, 23 μs, 20 μs, and 18 μs, respectively by the tube 400 mm.

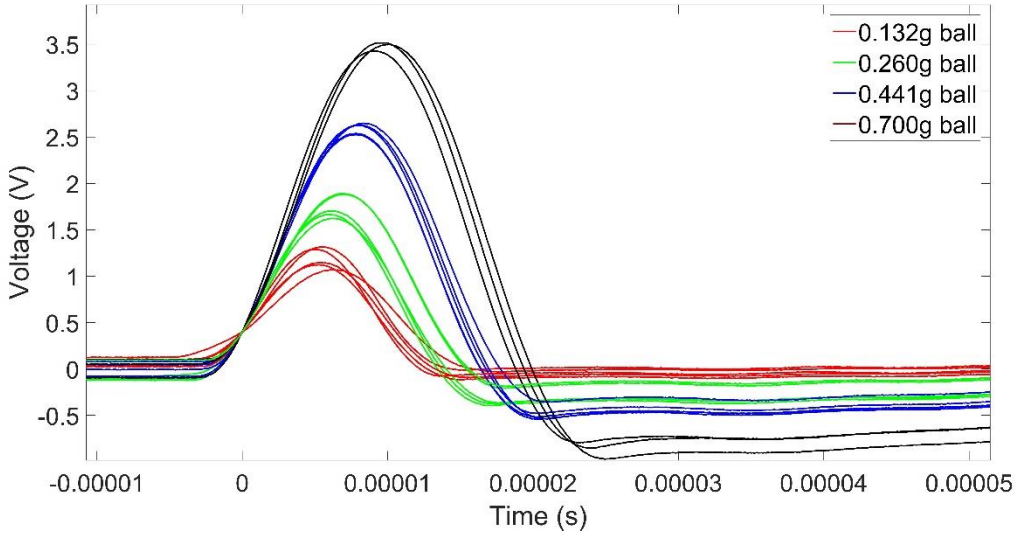

Figure 3.18: Calibration signal MSI PVDF Sensor (tube 400 mm).

In Figure 3.19, the average maximum voltages were 3 V with the ball of 0.700 g, 2.3 V with the ball of 0.441 g, 1.5 V with the ball of 0.260 g, and 1 V with the ball of 0.132 g, while the impact durations were 27 μs, 24 μs, 21 μs, and 18 μs, respectively by the tube 300mm.

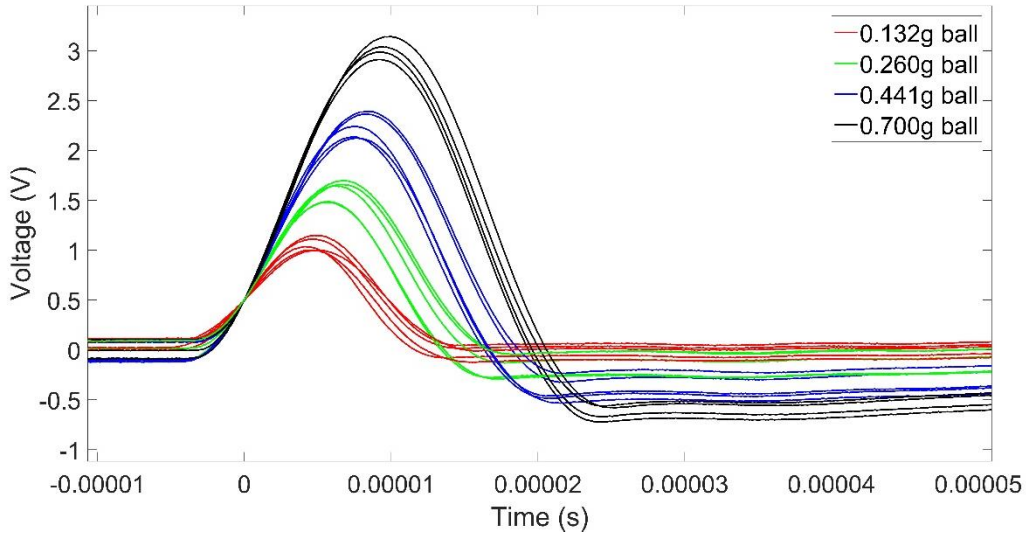

Figure 3.19: Calibration signal MSI PVDF Sensor (tube 300 mm).

In Figure 3.20, the tube for testing was 150 mm. The impact durations were 30 μs, μs27, 23 μs, 21 μs and the average maximum voltages were 2 V with the ball of 0.700 g, 1.4 V with the ball of 0.441 g, 0.95 V with the ball of 0.260 g, and 0.6 V with the ball of 0.132 g, respectively.

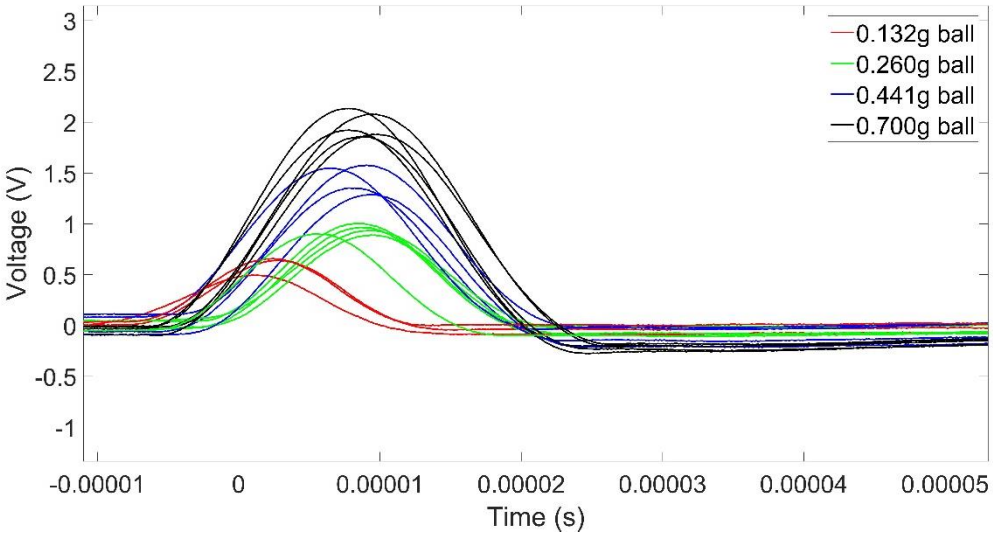

Figure 3.20: Calibration signal MSI PVDF Sensor (tube 150 mm).

4 RESULTS AND DISCUSSION

The output signal of the PVDF sensor from the ball drop is recorded with the different three tubes and four different ball weights. Based on these results, analysis is carried out to explain the sensitivity of the sensor, effect of size, and effect of protective layer. Also, testing with ultrasonic cavitation.

4.1 Effect of time duration and initial high in calibration

Figure 4.1 illustrates the relation between impact time duration and initial high for the two different PVDF sensor configurations. The results of the two PVDF films indicate that the impact time duration is a function of initial high. The increase of initial high and the mass impact, the decrease of impact time. On the other hand, it can be seen that for the TUL PVDF sensor the impact time duration is higher than the MSI PVDF sensor for the same initial high.

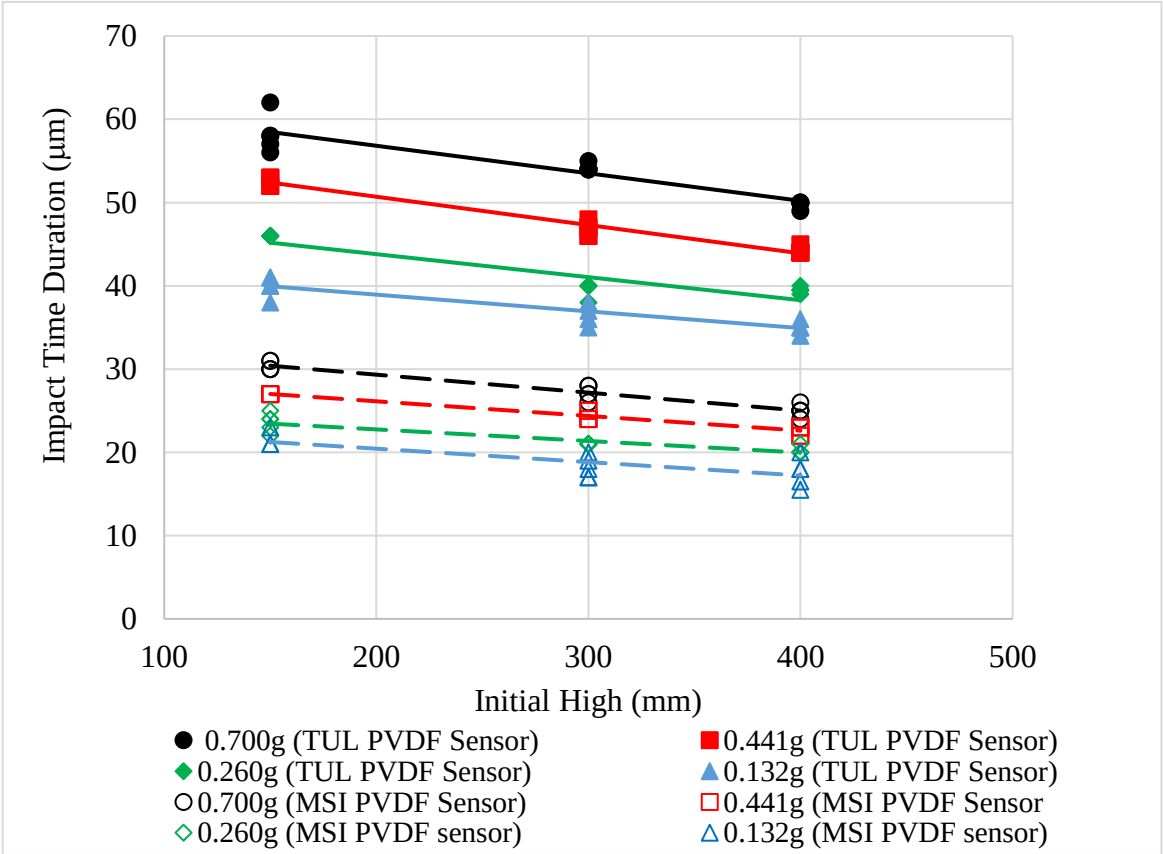

Figure 4.1: Impact time duration as a function of initial high for TUL and MSI sensor (12 mm × 10 mm).

4.2 Calibration results

The calibration curves in figure 4.2 to Figure 4.6 were plotted the maximum voltage Vs maximum impact load. The curve, demonstrating the relation between the maximum impact load with the sensor output voltage, is a linear increase. The sensitivity constant is proportional between the output voltage of the sensor and the maximum impact load. The linear least square method was used to calculate the sensitivity constant of the transducer. The sensitivity constant for TUL sensor (12 mm × 30 mm, 12 mm × 10 mm, 12 mm ×1 mm) are 0.013 V/N, 0.0262 V/N, 0.758 V/N and MSI sensor (12 mm × 30 mm, 12 mm × 10 mm) are 0.008 V/n ,and 0.0143 V/N, respectively and the R^2 is the value of the fitting line.

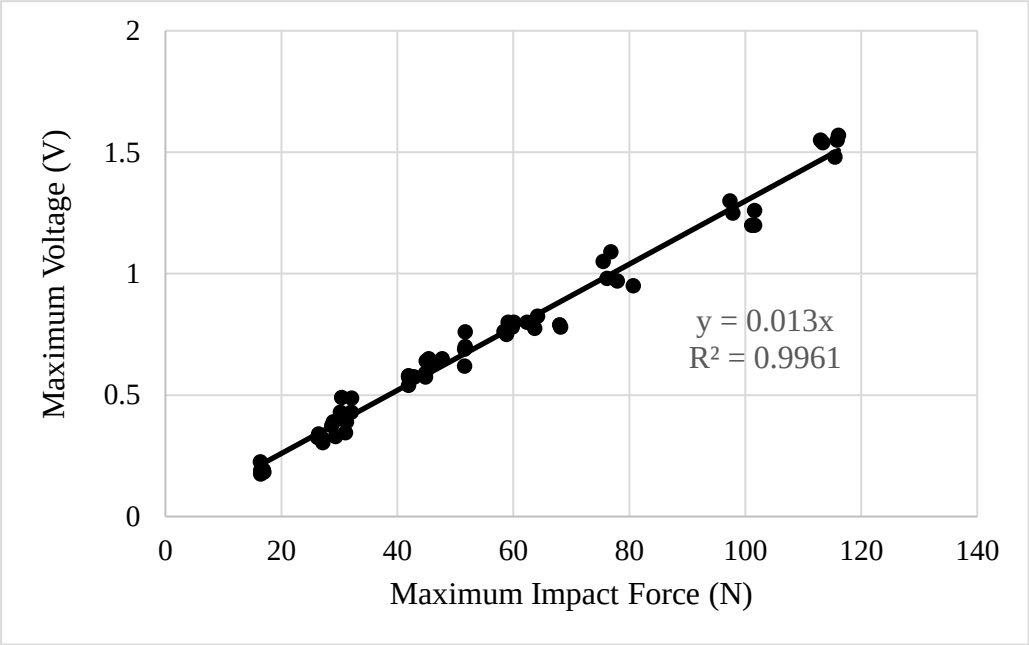

Figure 4.2: Calibration curve of TUL sensor with sensitive area 12 mm × 30 mm.

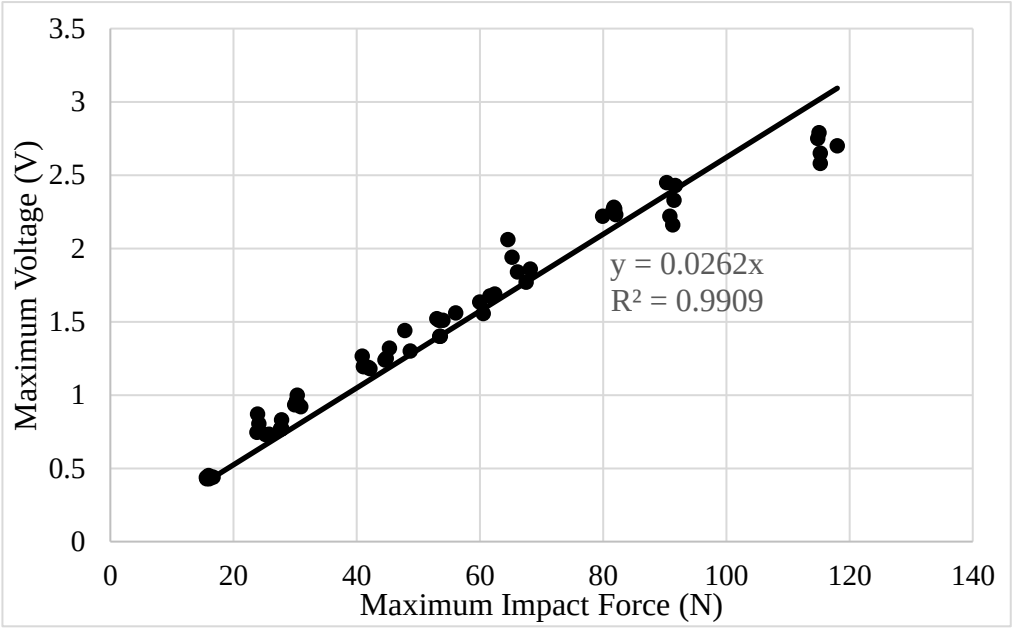

Figure 4.3: Calibration curve of TUL sensor with sensitive area 12 mm × 10 mm.

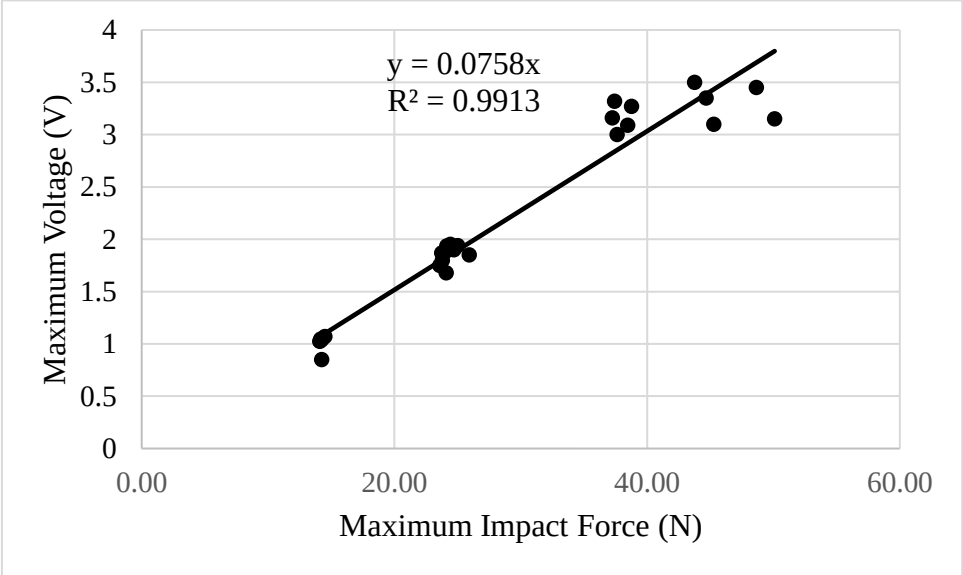

Figure 4.4: Calibration curve of TUL sensor with sensitive area 12 mm ×1 mm.

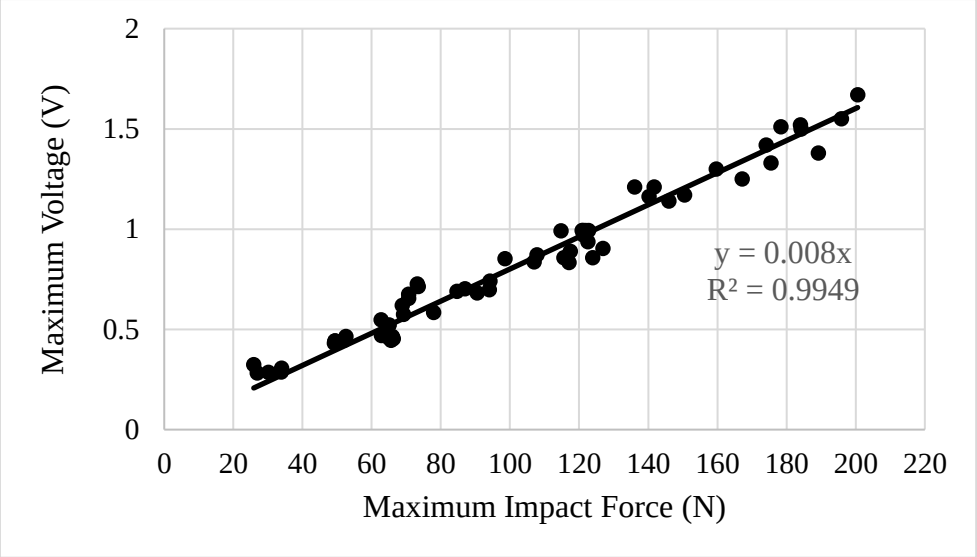

Figure 4.5: Calibration curve of MSI sensor with sensitive area 12 mm × 30 mm.

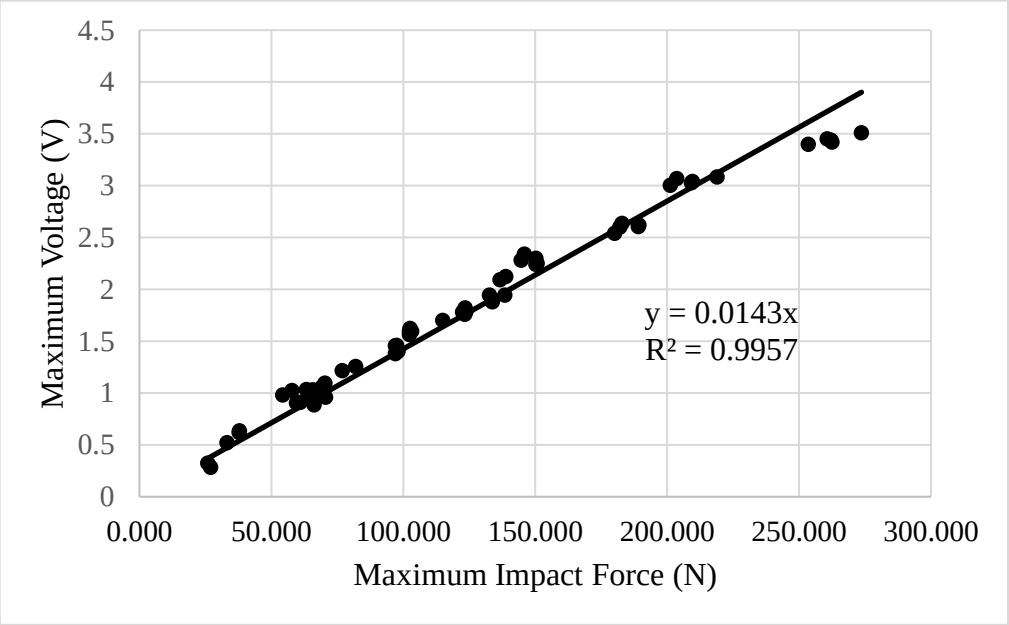

Figure 4.6: Calibration curve of MSI sensor with sensitive area 12mm × 10 mm.

Figure 4.7 illustrates that TUL sensors generate higher voltage than MSI sensors when applying the same impact load and sensitivity area of the sensor. It demonstrates the sensitivity constants of the TUL sensor are higher than the MSI sensor. It can be said that the TUL sensor is more suitable for measuring dynamic loading as cavitation than the MSI sensor.

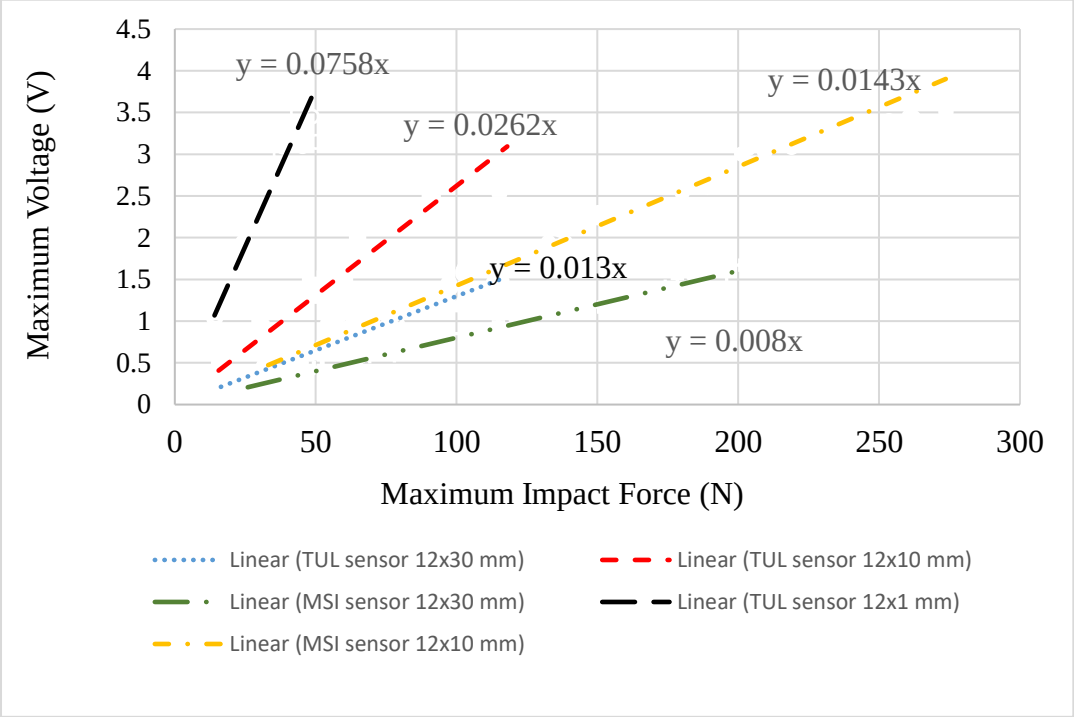

Figure 4.7: All calibration curve of PVDF sensor.

4.3 Effect of TUL PVDF sensor size

As seen in Figure 4.2 - 4.4, the maximum output voltage of a TUL PVDF sensor depends on the sensitive area. The small sensitive area of the sensor is generated the maximum output voltage more than the big area at the same impact load. This result is consistent with Soyama et al. [10] and MSI PVDF sensor. Table 6 shows that the sensitivity constant depends on the size of transducers. It can be seen that all PVDF sensors that the sensitivity increases with the decreasing of the active area of the sensor.

Table 7: Sensitivity contents with active area.

PVDF sensor	Active area (mm^2)	Sensitivity constants (V/N)
TUL Sensor (12x1)	12	0.0758
TUL Sensor (12x10)	120	0.0262
TUL Sensor (12x30)	360	0.0130

4.4 Effect of protective layer

The presence of a protective layer is used to avoid the sensor being damaged but also to change the sensor sensitivity. The sensor, which was used, had an active area of 120 mm^2, with one more layer of kapton tape added on the top of the sensor. The sensitivity constants for non-add, and one layer protective layer are 0,0262 V/N, and 0,0136 V/N, respectively, as shown in Figure 4.8. It is observed that as the protective layer thickness increases, the sensitivity constants decrease at a particular pressure. Hujer et al. [25] reported similar results.

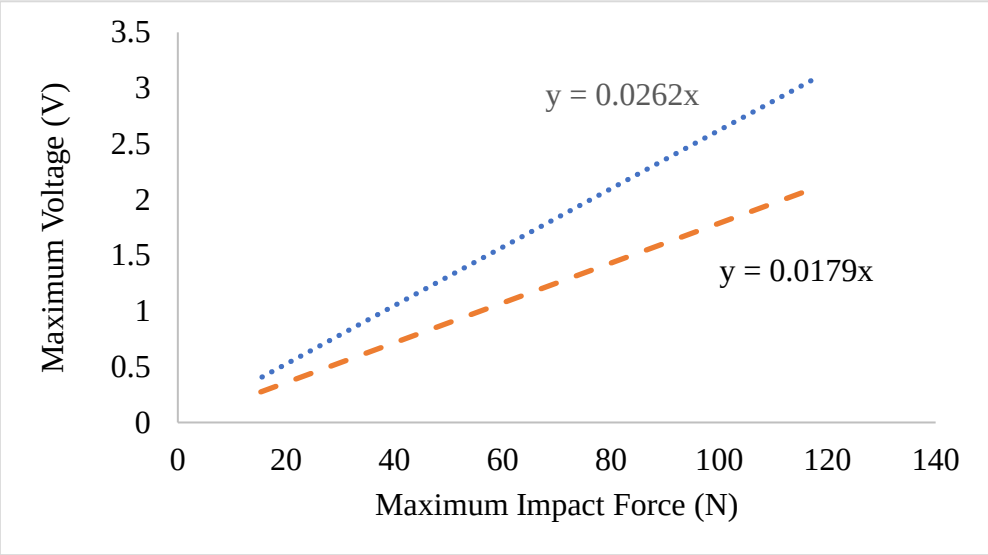

Figure 4.8: Calibration curves with effect of protective layer.

4.5 Testing with ultrasonic cavitation

Ultrasonic device (UIP1000hdT - Hielscher) is used for this testing. This device is attached to a horn and the vibrating frequency at 20 kHz with amplitude 90% of 57 μm. The PVDF sensor is set up under the horn 3.5 mm. The sensor is sunk in the water contained in the container. Figure 4.9 illustrates the signal output of the TUL PVDF sensor (12 mm x 10 mm) affixed to the metal plate in the form of a voltage (V) vs. time (s). The highest voltage of bubble collapse is 1.8 V. The shape of the curve by each bubble collapse is similar to the curve of calibration. Also, this signal shows the similarity to the MSI PVDF signal data measured by Myka [28]. Thus, it demonstrates that the TUL PVDF is suitable for cavitation measurement.

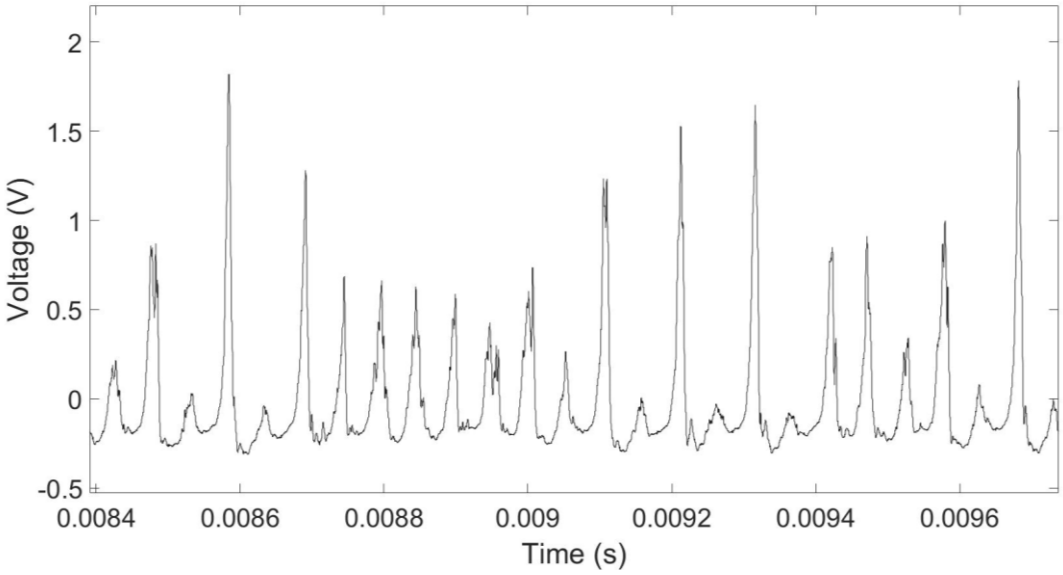

Figure 4.9: Signal from the TUL PVDF sensor tested ultrasonic cavitation.

5 CONCLUSION

The piezoelectric sensors were fabricated by a photolithography process with the positive and negative electrodes in different sizes of the sensor, while the Kapton tape was used as a protective layer, and rivets as the connection between sensor and wire.

The experiment was done by configurations TUL and MSI PVDF sensor mounted on the metal platform; meanwhile, the ball drop method was used to the calibration of the PVDF sensor. The impact time duration of the PVDF sensor was a function of the initial high ball drop. As a result, when the initial high and the mass of the ball increased, the impact duration time decreased. Furthermore, the maximum voltage gathered from the PVDF film showed a linear relationship with the maximum impact force. A comparison of the sensitivity constant of the TUL and MSI PVDF sensor was made. The results showed that the sensitivity constant of TUL sensor is higher than the sensitivity constant of MSI sensor. What's more, the different sizes of the sensitivity area of the TUL PVDF were also tested. The results indicated that the decrease in the active area of the sensor would increase the sensitivity constant of the sensor. The influence of the thickness of the protective layers for the TUL PVDF sensor was also investigated. It was also observed that the sensitivity constants depended on the thickness of the protective layers when the protective layer thickness increased, the sensitivity constants decreased. The sensor was tested with the ultrasonic cavitation; therefore, the sensor could be used to measure the cavitation.

6 REFERENCES

[1] K.-H. Kim, G. CHAHINE, J.-P. FRANC and A. KARIMI, Advanced Experimental and Numerical Techniques for Cavitation Erosion Prediction, vol. 106, Dordrecht: Springer Science+Business Media,, 2014.

[2] J.-P. Franc and M. Jean-Marie, Fundamentals of Cavitation, Dordrecht: Kluwer Academic Publishers, 2004.

[3] R. T. Knapp, J. W. Daily and F. G. Hammitt, Cavitation, New York: McGraw-Hill, 1970.

[4] S. NIRALI, "A REPORT ON CAVITATION," researchgate, 2014.

[5] S. I.Green (eds.), Fluid Vortices (Fluid Mechanics and Its Applications), Springer; 1995 edition (March 31, 1995), 1995.

[6] Y. Shah, A. Pandit and V. Moholkar , Cavitation Reaction Engineering (The Plenum Chemical Engineering Series), Springer, 1999.

[7] E. Ayli, "Cavitation in Hydraulic Turbines," *International Journal of Heat and Technology,* vol. 37, no. 1, pp. 334-344, 2019.

[8] Y. A. Pishchalnikov and O. A. Sapozhnikov, "Cavitation bubble cluster activity in the breakage of stones by shock wave lithotripsy," *The Journal of the Acoustical Society of America,* vol. 111, no. 5, pp. 24-61, 2002.

[9] C. . E. Brennen, "Cavitation in medicine," *Interface Focus,* vol. 5, no. 5, 2015.

[10] N. Asaithambi, P. Singha, M. Dwivedi and u. k. Singh, "Hydrodynamic cavitation and its application in food and beverage industry: A review," *Journal of Food Process Engineering,* 2019.

[11] P. R. Gogate and G. S. Bhosale, "Comparison of effectiveness of acoustic and hydrodynamic cavitation in combined treatment schemes for degradation of dye wastewaters," *Elsevier,* vol. 71, no. 1, pp. 59-69, 2013.

[12] J. P. Franc, L. d'Agostino and M. V. Salvetti, "Fulid Dynamics of Cavitaion and Cavitating Turbopumps".

[13] H. Kawai, "The Piezoelectricity of Poly (vinylidene Fluoride)," *Japanese Journal of Applied Physics,* vol. 8, no. 7, pp. 975-976, 1969.

[14] B. Bera and M. D. Sarka, "Piezoelectricity in PVDF and PVDF Based Piezoelectric Nanogenerator: A Concept," *IOSR Journal of Applied Physics,* vol. 9, no. 3, pp. 95-99, 2017.

[15] Z. Gaofeng, L. Yanming, L. Zhengfeng, C. Lujun, G. Shirui and S. Huichao, "A Flexible Thin Film Single-Point Force Sensor from PVDF Film," *Journal of Modern Mechanical Engineering and Technology,* pp. 47-55, 2018.

[16] I. Measurement Specialties, "Piezo Film Sensors Technical Manual," 2009.

[17] J. Cong, J. Jing, C. Chen and Z. Dai, "Development of a PVDF Sensor Array for Measurement of the Dynamic Pressure Field of the Blade Tip in an Axial Flow Compressor," *Sensors (Basel, Switzerland),* vol. 19, no. 6, p. 1404, 2019.

[18] Y. C. Wang and Y. W. Chen, "Application of piezoelectric PVDF film to the measurement of impulsive forces generated by cavitation bubble collapse near a solid boundary," *Experimental Thermal and Fluid Science,* vol. 32, no. 2, pp. 403-414, 2007.

[19] Y. Hu, W. Kang, Y. Fang, L. Xie, L. Qiu and T. Jin, "Piezoelectric Poly(vinylidene fluoride) (PVDF) Polymer-Based Sensor for Wrist Motion Signal Detection," *applied sciences,* vol. 8, no. 5, p. 836, 2018.

[20] J. Sirohi and I. Chopra, "Fundamental Understanding of Piezoelectric Strain Sensors," *Journal of Intelligent Material Systems and Structres,* vol. 11, pp. 246-257, 2000.

[21] B. MIKA, Design and Testing Of Piezoelectric Sensors, Texas A&M University, 2007.

[22] Q. Li, J. Xing, D. Shang and Y. Wang, "A Flow Velocity Measurement Method Based on a PVDF Piezoelectric Sensor," *Sensors (Basel, Switzerland),* vol. 19(7), p. 1657, 2019.

[23] D. Faust and R. Lakes, "Temperature and Substrate Dependence of Piezoelectric Sensitivity for PVDF Films," *Ferroelectrics,* vol. 481, pp. 1-9, 2015.

[24] Y. C. Wang, C.-H. Huang, Y.-C. Lee and a. H.-H. Tsai, "Development of a PVDF Sensor Array for Measurement of the Impulsive Pressure Generated by Cavitation Bubble Collapse," *Experiments in Fluids,* vol. 41, pp. 365-373, 2006.

[25] J. Hujer and M. Muller, "Calibration of PVDF Film Transducers for the Cavitation Impact Measurement," *EPJ Web of Conferences,* vol. 180, p. 02036, 2018.

[26] J. Hujer, J. Carrat, M. Muller and M. Riondet, "Impact load measurements with a PVDF pressure sensor in an erosive cavitating flow," *Journal of Physics: Conference Series,* vol. 656, no. 1, pp. 1-5, 2015.

[27] H. Soyama, A. Lichtarowicz, T. Momma and . E. J. Williams, "A New Calibration Method for Dynamically Loaded Transducers and Its Application to Cavitation Impact Measurement," *Journal of Fluids Engineering,* vol. 120, pp. 712-718, 1998.

[28] M. M. C. Duran, "Investigation of the Cavitation Aggressiveness Using PVDF Sensors," Technical University of Liberec, Liberec, 2018.

[29] K. Kotian, Detection of in-plane stress waves with Polyvinylidene Fluoride (PVDF) sensors, The Ohio State University, 2013.

[30] H. C. Buckland, I. Masters, J. A. Orme and T. Baker, "Cavitation inception and simulationin blade element momentum theory formodelling tidal stream turbines," *Journal of POWER AND ENERGY,* vol. 227, no. 4, pp. 479-485, 2013.

[31] M. S. Plesset and A. Prosperetti, "Bubble Dynamics and Cavitation," *Annual Review of Fluid Mechanics ,* vol. 9, no. 1, pp. 145-185, 1977.

[32] T. Connectivity, "TE Connectivity, LDT1-028K PIEZO SENSOR w/ Leads Attached," 2015.

[33] E. O. Aidoo, Material response on the cavitation bubble collapses, Technical University of Liberec, 2018.

[34] T. CONNECTIVITY, "TE CONNECTIVITY, METALLIZED PIEZO FILM SHEETS," TE.com/sensorsolutions, 2017.

[35] C. E. Brennen, "An Introduction to Cavitation Fundamentals," in *Cavitation: Turbo-machinery & Medical Applications*, University of Warwick, UK, 2011.

APPENDIX

Table A.1 Calibration data of the MSI PVDF sensor (Sensitive area 12 mm × 30 mm)

Trail	Mas of ball (g)	h_1 (mm)	h_2 (mm)	V_1 (m/s)	V_2 (m/s)	t_1 (μs)	t_2 (μs)	τ (μs)	U_{max} (N)	F_{max} (V)
1.1	0.700	400	168	2.80	1.82	995	1028	33	1.55	195.87
1.2	0.700	400	166	2.80	1.80	994	1029	35	1.50	184.24
1.3	0.700	400	165	2.80	1.80	995	1030	35	1.52	184.03
1.4	0.700	400	140	2.80	1.66	994	1029	35	1.51	178.35
1.5	0.700	400	162	2.80	1.78	995	1027	32	1.67	200.56
2.1	0.441	400	170	2.80	1.83	995	1025	30	1.21	136.06
2.2	0.441	400	171	2.80	1.83	994	1022	28	1.14	145.94
2.3	0.441	400	167	2.80	1.81	994	1023	29	1.16	140.25
2.4	0.441	400	176	2.80	1.86	994	1023	29	1.21	141.72
2.5	0.441	400	166	2.80	1.80	996	1023	27	1.17	150.47
3.1	0.260	400	178	2.80	1.87	995	1016	21	0.86	115.64
3.2	0.260	400	189	2.80	1.93	996	1017	21	0.83	117.05
3.3	0.260	400	158	2.80	1.76	996	1018	22	0.87	107.83
3.4	0.260	400	156	2.80	1.75	993	1017	24	0.85	98.60
3.5	0.260	400	190	2.80	1.93	995	1018	23	0.84	106.99
4.1	0.132	400	250	2.80	2.21	998	1015	17	0.58	77.90
4.2	0.132	400	242	2.80	2.18	998	1017	19	0.57	69.20
4.3	0.132	400	245	2.80	2.19	993	1014	21	0.55	62.78
4.4	0.132	400	230	2.80	2.12	994	1014	20	0.52	65.02
4.5	0.132	400	228	2.80	2.12	993	1013	20	0.52	64.90
5.1	0.700	300	104	2.43	1.43	994	1025	31	1.42	174.08
5.2	0.700	300	117	2.43	1.52	994	1027	33	1.25	167.20
5.3	0.700	300	125	2.43	1.57	993	1028	35	1.30	159.69
5.4	0.700	300	135	2.43	1.63	995	1025	30	1.38	189.17
5.5	0.700	300	128	2.43	1.58	995	1027	32	1.33	175.47
6.1	0.441	300	132	2.43	1.61	992	1023	31	0.99	114.81
6.2	0.441	300	156	2.43	1.75	993	1023	30	0.99	122.76
6.3	0.441	300	146	2.43	1.69	993	1023	30	0.99	121.09
6.4	0.441	300	145	2.43	1.69	993	1023	30	0.99	120.92
6.5	0.441	300	150	2.43	1.72	993	1023	30	0.99	121.76
7.1	0.260	300	122	2.43	1.55	993	1023	30	0.62	68.87
7.2	0.260	300	139	2.43	1.65	993	1023	30	0.66	70.68
7.3	0.260	300	165	2.43	1.80	993	1023	30	0.73	73.24
7.4	0.260	300	163	2.43	1.79	992	1023	31	0.68	70.69
7.5	0.260	300	168	2.43	1.82	993	1023	30	0.71	73.52
8.1	0.132	300	195	2.43	1.96	992	1014	22	0.46	52.59
8.2	0.132	300	180	2.43	1.88	992	1015	23	0.44	49.42
8.3	0.132	300	180	2.43	1.88	993	1016	23	0.44	49.42
8.4	0.132	300	185	2.43	1.91	996	1018	22	0.45	51.98
8.5	0.132	300	177	2.43	1.86	992	1015	23	0.43	49.24
9.1	0.700	150	74	1.72	1.20	993	1026	33	0.86	123.90

9.2	0.700	150	76	1.72	1.22	993	1028	35	0.89	117.47
9.3	0.700	150	81	1.72	1.26	994	1028	34	0.94	122.55
9.4	0.700	150	77	1.72	1.23	992	1026	34	0.97	121.25
9.5	0.700	150	83	1.72	1.28	992	1025	33	0.90	126.92
10.1	0.441	150	81	1.72	1.26	992	1023	31	0.69	84.68
10.2	0.441	150	79	1.72	1.24	992	1022	30	0.70	87.04
10.3	0.441	150	83	1.72	1.28	994	1022	28	0.74	94.24
10.4	0.441	150	81	1.72	1.26	994	1023	29	0.68	90.52
10.5	0.441	150	82	1.72	1.27	990	1018	28	0.70	93.99
11.1	0.260	150	90	1.72	1.33	998	1022	24	0.47	65.96
11.2	0.260	150	92	1.72	1.34	1000	1024	24	0.45	66.28
11.3	0.260	150	99	1.72	1.39	1000	1025	25	0.46	64.67
11.4	0.260	150	88	1.72	1.31	998	1022	24	0.45	65.64
11.5	0.260	150	87	1.72	1.31	998	1023	25	0.47	62.86
12.1	0.132	150	95	1.72	1.37	994	1018	24	0.29	33.89
12.2	0.132	150	96	1.72	1.37	994	1018	24	0.31	33.97
12.3	0.132	150	95	1.72	1.37	995	1022	27	0.29	30.12
12.4	0.132	150	10	1.72	0.44	997	1019	22	0.32	25.90
12.5	0.132	150	92	1.72	1.34	990	1020	30	0.28	26.92

Table A.2 Calibration data of the MSI PVDF sensor (Sensitive area 12 mm × 10 mm)

Trail	Mas of ball (g)	h_1 (mm)	h_2 (mm)	V_1 (m/s)	V_2 (m/s)	t_1 (μs)	t_2 (μs)	τ (μs)	U_{max} (N)	F_{max} (V)
1.1	0.700	400	181	2.80	1.88	98	123	25	3.42	262.41
1.2	0.700	400	185	2.80	1.91	98	124	26	3.40	253.43
1.3	0.700	400	182	2.80	1.89	98	122	24	3.51	273.65
1.4	0.700	400	175	2.80	1.85	98	123	25	3.45	260.65
1.5	0.700	400	180	2.80	1.88	98	123	25	3.44	262.12
2.1	0.441	400	197	2.80	1.97	97	120	23	2.64	182.82
2.2	0.441	400	188	2.80	1.92	98	120	22	2.62	189.31
2.3	0.441	400	193	2.80	1.95	97	120	23	2.60	182.05
2.4	0.441	400	183	2.80	1.89	98	121	23	2.54	180.09
2.5	0.441	400	187	2.80	1.92	98	120	22	2.61	189.10
3.1	0.260	400	193	2.80	1.95	97	117	20	1.82	123.43
3.2	0.260	400	196	2.80	1.96	98	118	20	1.79	123.82
3.3	0.260	400	192	2.80	1.94	97	117	20	1.76	123.30
3.4	0.260	400	173	2.80	1.84	97	118	21	1.70	114.99
3.5	0.260	400	186	2.80	1.91	98	118	20	1.78	122.51
4.1	0.132	400	204	2.80	2.00	97.5	114	16.5	1.22	76.83
4.2	0.132	400	205	2.80	2.01	97.5	113	15.5	1.26	81.87
4.3	0.132	400	202	2.80	1.99	97	115	18	1.10	70.29
4.4	0.132	400	201	2.80	1.99	96	116	20	1.04	63.19
4.5	0.132	400	186	2.80	1.91	97	115	18	1.06	69.11
5.1	0.700	300	130	2.43	1.60	996	1024	28	3.00	201.16
5.2	0.700	300	138	2.43	1.65	996	1024	28	3.07	203.58
5.3	0.700	300	132	2.43	1.61	997	1024	27	3.03	209.24
5.4	0.700	300	137	2.43	1.64	997	1023	26	3.09	218.92
5.5	0.700	300	133	2.43	1.62	997	1024	27	3.04	209.56
6.1	0.441	300	143	2.43	1.68	997	1022	25	2.28	144.69
6.2	0.441	300	149	2.43	1.71	996	1021	25	2.34	145.91
6.3	0.441	300	141	2.43	1.66	996	1020	24	2.24	150.28
6.4	0.441	300	143	2.43	1.68	996	1020	24	2.25	150.72
6.5	0.441	300	141	2.43	1.66	997	1021	24	2.30	150.28
7.1	0.260	300	149	2.43	1.71	997	1018	21	1.60	102.41
7.2	0.260	300	148	2.43	1.70	997	1018	21	1.57	102.27
7.3	0.260	300	150	2.43	1.72	997	1018	21	1.63	102.55
7.4	0.260	300	154	2.43	1.74	996	1017	21	1.60	103.12
7.5	0.260	300	148	2.43	1.70	996	1017	21	1.60	102.27
8.1	0.132	300	144	2.43	1.68	997	1014	17	1.03	63.78
8.2	0.132	300	166	2.43	1.80	997	1014	17	1.03	65.70
8.3	0.132	300	145	2.43	1.69	995	1015	20	0.98	54.29
8.4	0.132	300	153	2.43	1.73	996	1015	19	1.03	57.78
8.5	0.132	300	152	2.43	1.73	996	1014	18	0.91	60.91
9.1	0.700	150	81	1.72	1.26	994	1024	30	2.13	138.89
9.2	0.700	150	79	1.72	1.24	995	1026	31	1.88	133.70
9.3	0.700	150	80	1.72	1.25	995	1025	30	1.95	138.52

9.4	0.700	150	75	1.72	1.21	995	1025	30	2.09	136.67
9.5	0.700	150	76	1.72	1.22	993	1024	31	1.95	132.62
10.1	0.441	150	84	1.72	1.28	995	1022	27	1.41	97.98
10.2	0.441	150	80	1.72	1.25	997	1024	27	1.38	96.97
10.3	0.441	150	80	1.72	1.25	996	1023	27	1.46	96.97
10.4	0.441	150	84	1.72	1.28	994	1021	27	1.40	97.98
10.5	0.441	150	82	1.72	1.27	994	1021	27	1.46	97.47
11.1	0.260	150	83	1.72	1.28	997	1021	24	0.98	64.82
11.2	0.260	150	86	1.72	1.30	994	1018	24	0.94	65.31
11.3	0.260	150	82	1.72	1.27	998	1020	22	0.96	70.53
11.4	0.260	150	75	1.72	1.21	998	1021	23	0.89	66.21
11.5	0.260	150	67	1.72	1.15	997	1022	25	0.90	59.53
12.1	0.132	150	70	1.72	1.17	987	1010	23	0.52	33.14
12.2	0.132	150	86	1.72	1.30	993	1014	21	0.64	37.90
12.3	0.132	150	85	1.72	1.29	993	1014	21	0.62	37.80

Table A.3 Calibration data of the TUL PVDF sensor (Sensitive area 12 mm × 30 mm)

Trail	Mas of ball (g)	h_1 (mm)	h_2 (mm)	V_1 (m/s)	V_2 (m/s)	t_1 (μs)	t_2 (μs)	τ (μs)	U_{max} (V)	F_{max} (N)
1.1	0.700	400	89	2.80	1.32	994	1044	50	1.48	115.44
1.2	0.700	400	88	2.80	1.31	994	1045	51	1.55	112.97
1.3	0.700	400	90	2.80	1.33	994	1045	51	1.54	113.38
1.4	0.700	400	92	2.80	1.34	995	1045	50	1.57	116.06
1.5	0.700	400	91	2.80	1.34	994	1044	50	1.55	115.85
2.1	0.441	400	87	2.80	1.31	992.5	1039	47	0.97	77.92
2.2	0.441	400	85	2.80	1.29	992	1039	47	1.09	76.81
2.3	0.441	400	86	2.80	1.30	992.5	1040	48	0.98	76.14
2.4	0.441	400	87	2.80	1.31	993	1041	48	1.05	75.48
2.5	0.441	400	88	2.80	1.31	993	1038	45	0.95	80.66
3.1	0.260	400	82	2.80	1.27	993	1034	41	0.69	51.62
3.2	0.260	400	82	2.80	1.27	993	1034	41	0.62	51.62
3.3	0.260	400	78	2.80	1.24	990	1034	44	0.65	47.73
3.4	0.260	400	83	2.80	1.28	993	1034	41	0.70	51.72
3.5	0.260	400	83	2.80	1.28	993	1034	41	0.76	51.72
4.1	0.132	400	75	2.80	1.21	991	1024	33	0.49	32.12
4.2	0.132	400	74	2.80	1.20	990	1023	33	0.43	32.05
4.3	0.132	400	77	2.80	1.23	989	1024	35	0.49	30.40
4.4	0.132	400	73	2.80	1.20	990	1025	35	0.43	30.16
4.5	0.132	400	73	2.80	1.20	990	1024	34	0.42	31.04
5.1	0.700	300	65	2.43	1.13	994	1043	49	1.26	101.58
5.2	0.700	300	65	2.43	1.13	994	1043	49	1.20	101.58
5.3	0.700	300	63	2.43	1.11	994	1043	49	1.20	101.08
5.4	0.700	300	66	2.43	1.14	993	1044	51	1.25	97.84
5.5	0.700	300	64	2.43	1.12	993	1044	51	1.30	97.36
6.1	0.441	300	55	2.43	1.04	992	1040	48	0.77	63.67
6.2	0.441	300	55	2.43	1.04	992	1041	49	0.80	62.37
6.3	0.441	300	58	2.43	1.07	992	1040	48	0.82	64.18
6.4	0.441	300	65	2.43	1.13	993	1039	46	0.78	68.17
6.5	0.441	300	64	2.43	1.12	993	1039	46	0.79	68.00
7.1	0.260	300	63	2.43	1.11	991	1032	41	0.59	44.87
7.2	0.260	300	64	2.43	1.12	991	1032	41	0.64	44.98
7.3	0.260	300	63	2.43	1.11	991	1032	41	0.57	44.87
7.4	0.260	300	63	2.43	1.11	991	1031	40	0.63	45.99
7.5	0.260	300	58	2.43	1.07	992	1032	40	0.65	45.41
8.1	0.132	300	58	2.43	1.07	989	1023	34	0.31	27.12
8.2	0.132	300	57	2.43	1.06	988	1023	35	0.32	26.28
8.3	0.132	300	58	2.43	1.07	989	1024	35	0.33	26.35
8.4	0.132	300	58	2.43	1.07	989	1023	34	0.32	27.12
8.5	0.132	300	59	2.43	1.08	988	1023	35	0.34	26.42
9.1	0.700	150	34	1.72	0.82	994	1054	60	0.80	59.09
9.2	0.700	150	33	1.72	0.80	994	1054	60	0.75	58.80
9.3	0.700	150	33	1.72	0.80	993	1052	59	0.78	59.80

9.4	0.700	150	35	1.72	0.83	993	1054	61	0.76	58.39
9.5	0.700	150	34	1.72	0.82	993	1052	59	0.80	60.09
10.1	0.441	150	33	1.72	0.80	992	1044	52	0.58	42.75
10.2	0.441	150	33	1.72	0.80	992	1045	53	0.54	41.94
10.3	0.441	150	34	1.72	0.82	992	1044	52	0.58	42.95
10.4	0.441	150	33	1.72	0.80	991	1044	53	0.58	41.94
10.5	0.441	150	33	1.72	0.80	991	1044	53	0.58	41.94
11.1	0.260	150	30	1.72	0.77	992	1036	44	0.33	29.34
11.2	0.260	150	33	1.72	0.80	992	1034	42	0.39	31.20
11.3	0.260	150	32	1.72	0.79	992	1034	42	0.35	31.05
11.4	0.260	150	30	1.72	0.77	991	1036	45	0.38	28.69
11.5	0.260	150	32	1.72	0.79	991	1036	45	0.39	28.98
12.1	0.132	150	25	1.72	0.70	991	1030	39	0.23	16.35
12.2	0.132	150	26	1.72	0.71	991	1030	39	0.18	16.45
12.3	0.132	150	26	1.72	0.71	991	1030	39	0.2	16.45
12.4	0.132	150	27	1.72	0.73	990	1028	38	0.18	16.97
12.5	0.132	150	26	1.72	0.71	990	1028	38	0.19	16.88

Table A.4 Calibration data of the TUL PVDF sensor (Sensitive area 12 mm × 10 mm)

Trail	Mas of ball (g)	h_1 (mm)	h_2 (mm)	V_1 (m/s)	V_2 (m/s)	t_1 (μs)	t_2 (μs)	τ (μs)	U_{max} (V)	F_{max} (N)
1.1	0.700	400	90	2.80	1.33	995	1044	49	2.7	118.01
1.2	0.700	400	88	2.80	1.31	995	1045	50	2.65	115.23
1.3	0.700	400	87	2.80	1.31	995	1045	50	2.79	115.02
1.4	0.700	400	88	2.80	1.31	995	1045	50	2.58	115.23
1.5	0.700	400	86	2.80	1.30	995	1045	50	2.75	114.81
2.1	0.441	400	85	2.80	1.29	995	1039	44	2.23	82.04
2.2	0.441	400	83	2.80	1.28	995	1039	44	2.28	81.74
2.3	0.441	400	84	2.80	1.28	995	1039	44	2.27	81.89
2.4	0.441	400	82	2.80	1.27	995	1039	44	2.26	81.58
2.5	0.441	400	83	2.80	1.28	995	1040	45	2.22	79.92
3.1	0.260	400	80	2.80	1.25	993.5	1033	39.5	1.51	53.37
3.2	0.260	400	82	2.80	1.27	993.5	1033	39.5	1.4	53.58
3.3	0.260	400	79	2.80	1.24	994	1033	39	1.51	53.95
3.4	0.260	400	81	2.80	1.26	993.5	1033	39.5	1.4	53.48
3.5	0.260	400	83	2.80	1.28	994	1034	40	1.52	53.01
4.1	0.132	400	74	2.80	1.20	992	1027	35	0.96	30.22
4.2	0.132	400	74	2.80	1.20	992	1027	35	0.96	30.22
4.3	0.132	400	76	2.80	1.22	993	1028	35	1.00	30.34
4.4	0.132	400	71	2.80	1.18	993	1027	34	0.92	30.92
4.5	0.132	400	83	2.80	1.28	992	1028	36	0.93	29.90
5.1	0.700	300	59	2.43	1.08	992	1046	54	2.22	90.793
5.2	0.700	300	61	2.43	1.09	992	1046	54	2.16	91.262
5.3	0.700	300	64	2.43	1.12	992	1047	55	2.45	90.279
5.4	0.700	300	62	2.43	1.10	992	1046	54	2.33	91.493
5.5	0.700	300	63	2.43	1.11	992	1046	54	2.43	91.723
6.1	0.441	300	60	2.43	1.08	992	1040	48	2.06	64.516
6.2	0.441	300	56	2.43	1.05	992	1039	47	1.94	65.199
6.3	0.441	300	61	2.43	1.09	992	1039	47	1.84	66.058
6.4	0.441	300	65	2.43	1.13	992	1038	46	1.86	68.171
6.5	0.441	300	61	2.43	1.09	992	1038	46	1.77	67.494
7.1	0.260	300	58	2.43	1.07	992	1030	38	1.44	47.797
7.2	0.260	300	55	2.43	1.04	991	1028	37	1.30	48.696
7.3	0.260	300	53	2.43	1.02	990	1030	40	1.25	44.796
7.4	0.260	300	57	2.43	1.06	990	1030	40	1.32	45.287
7.5	0.260	300	51	2.43	1.00	990	1030	40	1.24	44.543
8.1	0.132	300	50	2.43	0.99	988	1023	35	0.73	25.771
8.2	0.132	300	52	2.43	1.01	988	1024	36	0.73	25.199
8.3	0.132	300	52	2.43	1.01	988	1026	38	0.87	23.872
8.4	0.132	300	51	2.43	1.00	987	1025	38	0.745	23.805
8.5	0.132	300	46	2.43	0.95	988	1025	37	0.805	24.089
9.1	0.700	150	32	1.72	0.79	992	1049	57	1.675	61.60
9.2	0.700	150	31	1.72	0.78	992	1048	56	1.690	62.39
9.3	0.700	150	30	1.72	0.77	993	1051	58	1.635	59.93

9.4	0.700	150	32	1.72	0.79	993	1051	58	1.555	60.54
9.5	0.700	150	30	1.72	0.77	992	1054	62	1.560	56.06
10.1	0.441	150	30	1.72	0.77	992	1044	52	1.180	42.11
10.2	0.441	150	29	1.72	0.75	992	1044	52	1.190	41.89
10.3	0.441	150	28	1.72	0.74	992	1045	53	1.265	40.88
10.4	0.441	150	29	1.72	0.75	992	1045	53	1.195	41.10
10.5	0.441	150	29	1.72	0.75	992	1045	53	1.194	41.10
11.1	0.260	150	28	1.72	0.74	991	1037	46	0.770	27.77
11.2	0.260	150	27	1.72	0.73	991	1037	46	0.767	27.62
11.3	0.260	150	28	1.72	0.74	991	1037	46	0.772	27.77
11.4	0.260	150	27	1.72	0.73	991	1037	46	0.770	27.62
11.5	0.260	150	28	1.72	0.74	992	1038	46	0.830	27.77
12.1	0.132	150	25	1.72	0.70	990	1030	40	0.450	15.94
12.2	0.132	150	26	1.72	0.71	989	1030	41	0.430	15.65
12.3	0.132	150	24	1.72	0.69	990	1028	38	0.440	16.69
12.4	0.132	150	26	1.72	0.71	990	1030	40	0.430	16.04
12.5	0.132	150	25	1.72	0.70	989	1030	41	0.438	15.56

Table A.5 Calibration data of the TUL PVDF sensor (Sensitive area 12 mm × 1 mm)

Trail	Mas of ball (g)	h_1 (mm)	h_2 (mm)	V_1 (m/s)	V_2 (m/s)	t_1 (μs)	t_2 (μs)	τ (μs)	U_{max} (V)	F_{max} (N)
1.1	0.260	300	65	2.43	1.13	992	1030	38	3.45	48.65
1.2	0.260	300	66	2.43	1.14	991	1028	37	3.15	50.09
1.3	0.260	300	57	2.43	1.06	990	1030	40	3.10	45.29
1.4	0.260	300	45	2.43	0.94	990	1030	40	3.50	43.75
1.5	0.260	300	52	2.43	1.01	990	1030	40	3.35	44.67
2.1	0.132	300	52	2.43	1.01	988	1023	35	1.85	25.92
2.2	0.132	300	49.5	2.43	0.99	988	1024	36	1.94	25.02
2.3	0.132	300	50	2.43	0.99	988	1026	38	1.87	23.74
2.4	0.132	300	48	2.43	0.97	987	1025	38	1.75	23.60
2.5	0.132	300	42	2.43	0.91	988	1025	37	1.80	23.79
3.1	0.441	150	31	1.72	0.78	996.5	1055	58.5	3.00	37.62
3.2	0.441	150	29	1.72	0.75	996.5	1055	58.5	3.16	37.24
3.3	0.441	150	30	1.72	0.77	996.5	1053	56.5	3.27	38.76
3.4	0.441	150	30	1.72	0.77	996.5	1055	58.5	3.32	37.43
3.5	0.441	150	28.5	1.72	0.75	996.5	1053	56.5	3.09	38.45
4.1	0.260	150	27	1.72	0.73	996	1048	52	1.95	24.43
4.2	0.260	150	28	1.72	0.74	995	1048	53	1.68	24.10
4.3	0.260	150	27	1.72	0.73	996	1048	52	1.93	24.43
4.4	0.260	150	29	1.72	0.75	996	1048	52	1.90	24.70
4.5	0.260	150	25	1.72	0.70	996	1048	52	1.94	24.16
5.1	0.132	150	25	1.72	0.70	996	1040	44	1.07	14.50
5.2	0.132	150	26	1.72	0.71	995	1040	45	1.04	14.25
5.3	0.132	150	26	1.72	0.71	995	1040	45	0.85	14.25
5.4	0.132	150	25	1.72	0.70	995	1040	45	1.05	14.17
5.5	0.132	150	24	1.72	0.69	995	1040	45	1.03	14.09

Table A.6 Calibration data of the TUL PVDF sensor added 1 Kapton tap (Sensitive area 12 mm × 10 mm)

Trail	Mas of ball (g)	h_1 (mm)	h_2 (mm)	V_1 (m/s)	V_2 (m/s)	t_1 (μs)	t_2 (μs)	τ (μs)	U_{max} (V)	F_{max} (N)
1.1	0.700	400	92	2.80	1.34	995	1055	60	1.85	96.72
1.2	0.700	400	92	2.80	1.34	995	1055	60	1.85	96.72
1.3	0.700	400	91	2.80	1.34	995	1055	60	1.80	96.54
1.4	0.700	400	94	2.80	1.36	995	1045	50	1.90	116.47
1.5	0.700	400	95	2.80	1.37	994	1044	50	1.95	116.67
2.1	0.441	400	94	2.80	1.36	995	1047	52	1.45	70.55
2.2	0.441	400	93	2.80	1.35	995	1047	52	1.20	70.43
2.3	0.441	400	92	2.80	1.34	995	1047	52	1.40	70.30
2.4	0.441	400	96	2.80	1.37	994	1047	53	1.35	69.46
2.5	0.441	400	97	2.80	1.38	995	1047	52	1.30	70.92
3.1	0.260	400	90	2.80	1.33	994	1040	46	1.05	46.69
3.2	0.260	400	91	2.80	1.34	994	1040	46	1.00	46.77
3.3	0.260	400	93	2.80	1.35	994	1040	46	0.86	46.94
3.4	0.260	400	92	2.80	1.34	994	1040	46	1.10	46.86
3.5	0.260	400	92	2.80	1.34	994	1039	45	0.95	47.90
4.1	0.132	400	81	2.80	1.26	992	1032	40	0.50	26.81
4.2	0.132	400	80	2.80	1.25	992	1032	40	0.58	26.76
4.3	0.132	400	86	2.80	1.30	992	1032	40	0.59	27.06
4.4	0.132	400	89	2.80	1.32	991	1032	41	0.60	26.55
4.5	0.132	400	82	2.80	1.27	991	1032	41	0.55	26.21
5.1	0.700	300	71	2.43	1.18	994	1055	61	1.35	82.77
5.2	0.700	300	73	2.43	1.20	994	1055	61	1.5	83.15
5.3	0.700	300	70	2.43	1.17	994	1055	61	1.3	82.58
5.4	0.700	300	73	2.43	1.20	994	1055	61	1.4	83.15
5.5	0.700	300	71	2.43	1.18	994	1055	61	1.5	82.77
6.1	0.441	300	73	2.43	1.20	994	1048	54	0.9	59.17
6.2	0.441	300	72	2.43	1.19	994	1048	54	1.2	59.04
6.3	0.441	300	72	2.43	1.19	994	1048	54	1.14	59.04
6.4	0.441	300	71	2.43	1.18	994	1048	54	1.05	58.90
6.5	0.441	300	66	2.43	1.14	994	1048	54	1.05	58.21
7.1	0.260	300	68	2.43	1.16	994	1040	46	0.84	40.48
7.2	0.260	300	70	2.43	1.17	994	1040	46	0.85	40.67
7.3	0.260	300	69	2.43	1.16	991	1041	50	0.91	37.33
7.4	0.260	300	70	2.43	1.17	991	1041	50	0.8	37.42
7.5	0.260	300	68	2.43	1.16	992	1040	48	0.822	38.80
8.1	0.132	300	65	2.43	1.13	991	1030	39	0.48	24.07
8.2	0.132	300	64	2.43	1.12	991	1030	39	0.5	24.01
8.3	0.132	300	68	2.43	1.16	991	1031	40	0.5	23.64
8.4	0.132	300	68	2.43	1.16	991	1031	40	0.49	23.64
8.5	0.132	300	65	2.43	1.13	991	1031	40	0.48	23.47
9.1	0.700	150	34	1.72	0.82	991	1057	66	1.24	53.71

9.2	0.700	150	30	1.72	0.77	991	1057	66	1.12	52.66
9.3	0.700	150	32	1.72	0.79	991	1057	66	1.19	53.20
9.4	0.700	150	33	1.72	0.80	992	1058	66	1.23	53.46
9.5	0.700	150	34	1.72	0.82	992	1058	66	1.20	53.71
10.1	0.441	150	34	1.72	0.82	990.5	1050	59.5	0.87	37.54
10.2	0.441	150	31	1.72	0.78	990.5	1050	59.5	0.87	36.99
10.3	0.441	150	33	1.72	0.80	991	1050	59	0.85	37.67
10.4	0.441	150	33	1.72	0.80	991	1050	59	0.92	37.67
10.5	0.441	150	32	1.72	0.79	991	1050	59	0.92	37.49
11.1	0.260	150	33	1.72	0.80	989	1042	53	0.57	24.73
11.2	0.260	150	35	1.72	0.83	985	1040	55	0.48	24.05
11.3	0.260	150	31	1.72	0.78	989	1042	53	0.52	24.48
11.4	0.260	150	35	1.72	0.83	989	1042	53	0.51	24.96
11.5	0.260	150	36	1.72	0.84	989	1042	53	0.54	25.08
12.1	0.132	150	35	1.72	0.83	987	1030	43	0.29	15.62
12.2	0.132	150	34.5	1.72	0.82	987	1030	43	0.29	15.58
12.3	0.132	150	35	1.72	0.83	987	1030	43	0.29	15.62
12.4	0.132	150	36	1.72	0.84	987	1031	44	0.29	15.34
12.5	0.132	150	34	1.72	0.82	987	1030	43	0.29	15.55